Bull Volcanol (2006) 68: 611–630
DOI 10.1007/s00445-005-0035-4

RESEARCH ARTICLE

Sylvie Vergniolle · Jacqueline Caplan-Auerbach

Basaltic thermals and Subplinian plumes: Constraints from acoustic measurements at Shishaldin volcano, Alaska

Received: 24 March 2004 / Accepted: 31 August 2005 / Published online: 11 February 2006

Abstract The 1999 basaltic eruption of Shishaldin volcano (Alaska, USA) included both Strombolian and Subplinian activity, as well as a "pre-Subplinian" phase interpreted as the local coalescence within a long foam in the conduit. Although few visual observations were made of the eruption, a great deal of information regarding gas velocity, gas flux at the vent and plume height may be inferred by using acoustic recordings of the eruption. By relating acoustic power to gas velocity, a time series of gas velocity is calculated for the Subplinian and pre-Subplinian phases. These time series show trends in gas velocity that are interpreted as plumes or, for those signals lasting only a short time, thermals. The Subplinian phase is shown to be composed of a thermal followed by five plumes with a total expelled gas volume of $\approx 1.5 \times 10^7$ m^3.

The initiation of the Subplinian activity is probably related to the arrival of a large overpressurised bubble close to the top of the magma column. A gradual increase in low-frequency (0.01–0.5 Hz) signal prior to this "trigger bubble" may be due to the rise of the bubble in the conduit. This delay corresponds to a reservoir located at ≈3.9 km below the surface, in good agreement with studies on other volcanoes.

The presence of two thermal phases is also identified in the middle of the pre-Subplinian phase with a total gas release of $\approx 4.3 \times 10^6$ m^3 and $\approx 3.6 \times 10^6$ m^3. Gas velocity at the vent is found to be ≈ 82 m.s^{-1} and ≈ 90 m.s^{-1} for the Subplinian plumes and the pre-Subplinian thermals respectively.

The agreement is very good between estimates of the gas flux from modelling the plume height and those obtained from acoustic measurements, leading to a new method by which eruption physical parameters may be quantified. Furthermore, direct measurements of gas velocity can be used for better estimates of the SO_2 flux released during the eruption.

Keywords Eruption dynamics · Basaltic plume · Basaltic thermal · Acoustic measurements · Shishaldin volcano · Alaska · Subduction zone

Editorial responsibility: J. Stix

S. Vergniolle (✉)
Laboratoire de Dynamique des Systèmes Géologiques,
Institut de Physique du Globe de Paris,
4 Place Jussieu,
75252 Paris Cedex 05, France
e-mail: vergniolle@ipgp.jussieu.fr
Tel.: +33-1-44272477
Fax: +33-1-44272481

Present address:
J. Caplan-Auerbach
Western Washington University,
Bellingham,
WA, USA
e-mail: jackie@geol.wwu.edu

Introduction

Explosive volcanic eruptions, those that produce ash plumes rather than lava flows, may be instigated by a number of processes. One possibility is that gaseous magma rises beneath a caprock, and it is the pressure release caused by caprock failure that generated an intense episode of bubble nucleation and growth (e.g. Sparks et al. 1997; Mader 1998). Alternatively, ash columns may be generated due to the interaction of magma with groundwater. Finally, explosive eruptions columns may result from the large gas content of the magma itself. In silicic magmas, the water content may be between 3 and 5 wt% (Sparks et al. 1997; Mader 1998). Less silicic magma can sometimes produce small scale plumes, as during Vulcanian explosions but the formation of a large purely magmatic plume is very rare for basalts, due to the relatively low water content (less than 1 wt%) (Zhang et al. 1997). However low-MgO high-Al_2O_3 basalts, which are common in subduction zones, have been found to be rich in water, up to 4 to 6 wt% (Sisson and Grove 1993; Johnson et al. 1994; Wallace and Anderson 2000). At Shishaldin, fluid inclusions show that the pre-eruptive H_2O content of this magma is low (≤1.5 wt%) (Stelling et al. 2002). While chemical measurements of melt inclusions represents local conditions prevailing at the phenocrysts

formation, the initial volatile content can be very underestimated if degassing has occurred (Wallace 2005). This is indeed the case at Shishaldin, where degassing was reported as significant prior to the eruption (Stelling et al. 2002).

Although some of the physical processes of plume formation have been constrained by laboratory experiments (Phillips et al. 1995; Mader et al. 1996; Zhang et al. 1997) or by numerical modelling (Alidibirov 1994; Massol and Jaupart 1999), several important unknowns remain. A crucial means of studying eruption columns and the mechanisms that promote their growth is through geophysical measurements. However, few such data exist due to both the rarity of large plumes and the difficulty of instrumenting explosive eruptions.

A major parameter to be studied in volcanic plumes is the velocity of ejecta at the vent. Ballistics studies have been used in the past to constrain velocities at volcanic vents (Chouet et al. 1974; McGetchin et al. 1974; Ripepe et al. 1993) and radar measurements (Weill et al. 1992; Hort and Seyfried 1998; Dubosclard et al. 1999, 2004; Hort et al. 2003) have been a recent major improvement. This reliable technique may, however, be difficult to implement as equipment is both heavy and energy consuming.

In the last ten years, acoustic measurements have been performed on a number of active volcanoes. The first group of studies associates the sound radiated during eruptions to resonance of magma in the conduit and includes the propagation of sound waves in the magma and atmosphere (Buckingham and Garcés 1996; Garcés and McNutt 1997; Hagerty et al. 2000). The second class of studies relates the source of sound to eruption dynamics, such as a sudden uncorking of the volcano (Johnson et al. 1998; Johnson and Lees 2000), local coalescence within a foam (Vergniolle and Caplan-Auerbach 2004) and Strombolian bubble vibration (Vergniolle and Brandeis 1994, 1996; Vergniolle et al. 1996, 2004). In the last case, gas velocity and bubble radius, length and overpressure have been estimated at Stromboli (Italy) (Vergniolle and Brandeis 1996; Vergniolle et al. 1996) and Shishaldin (Vergniolle et al. 2004) volcanoes.

Microbarograph networks have also been used to detect eruptions at large distances (LePichon et al. 2005) and to estimate vent pressure for large eruptions (Morrissey and Chouet 1997a, b). These studies indicate that vent pressure ranges over two orders of magnitude, from ≈0.2 MPa during Strombolian explosions at Sakurajima (Japan) to the largest eruptions, ≈7.5 MPa at Mount St. Helens (USA), and ≥5 MPa at Pinatubo (Philippines) (Morrissey and Chouet 1997b). In contrast to Mount St. Helens, activity at Pinatubo built up gradually with smaller explosions and continuous gas emission before leading to the climatic eruption (Kanamori and Mori 1992; Hoblitt et al. 1996).

Very little is known about basaltic Subplinian activity, which has only been recognised at a few volcanoes, including Etna (Coltelli et al. 1995, 2000; Houghton et al. 2004), Masaya (Nicaragua), (Williams 1983) and Shishaldin (Nye et al. 2002; Caplan-Auerbach and McNutt 2003). Plumes generated by Vulcanian-type activity are considered thermals if the release of the pyroclast-gas mixture occurs on a time scale much less than the ascent of the plume, hence in pratice last less than ten minutes (Sparks et al. 1997). Although the rise of a thermal in the atmosphere (Fig. 8 in Nye et al. 2002) is similar in some ways to a Vulcanian explosion, a thermal is not initiated by a large overpressure. Because pressure and gas velocity are the key variables to model the flow of magma and gas at the vent, measuring these is the first step in improving our understanding of physical processes. Furthermore direct measurements of gas velocity can be used to convert the amount of SO_2 measured by COSPEC into a more accurate flux of SO_2, as the plume speed is the greatest source of error in most COSPEC measurements (Andres and Rose 1995).

In this paper, acoustic measurements are used to study the 1999 basaltic Subplinian eruption of Shishaldin volcano, Alaska, as well as two small thermals that occurred during the precursory phase of the eruption. Because the acoustic signal associated with these plumes is quite complex, detailed modelling of the source is difficult. Consequently, we propose a method by which gas velocity at the vent can be estimated from dimensionless analysis. In two other papers, we show how acoustic measurements can be interpreted, together with laboratory experiments, to unravel the physical processes at work during the pre-Subplinian and Subplinian basaltic activity of Shishaldin, both in the conduit (Vergniolle and Caplan-Auerbach, subm.) and in the reservoir (Vergniolle, subm.).

Description of eruptive activity

Shishaldin is among the most active volcanoes in Alaska, with ≈40 eruptions in the past 200 years (Nye et al. 2002). Its historical eruptions are composed of basalt and basaltic andesite and have typically been brief with formation of ash plumes (Nye et al. 2002). Although only eleven tephra layers as large as that of 1999 have been identified in deposits spanning the past 9000 years (Beget et al. 1998), basaltic ash plumes are the most characteristic type of Shishaldin eruptive activity.

Shishaldin is one of five volcanoes comprising Unimak Island, the easternmost island in the Aleutian arc. Unfortunately, Shishaldin cannot be seen from the nearest population center, False Pass (Fig. 1) due to the presence of the nearer volcanoes Round Top and Isanotski. As a consequence, visual observations are minimal and the Alaska Volcano Observatory (AVO) relies heavily on telemetered seismic data and satellite imagery for volcanic monitoring. No other data such as deformation or gas emissions, were collected during the eruption (Nye et al. 2002).

In 1997, a six-station seismic network was installed near Shishaldin (Fig. 1). Five of the stations are short period Mark Products L-4C instruments with natural period of 1 sec. Station SSLS is a Mark Products three component L-22 instrument with 0.5-sec natural period. A Setra 239 pressure sensor is co-located with station SSLN on the volcano's north flank at 6.5 km from the vent. Details about the pressure sensor installation and response are included in another paper (Vergniolle et al. 2004).

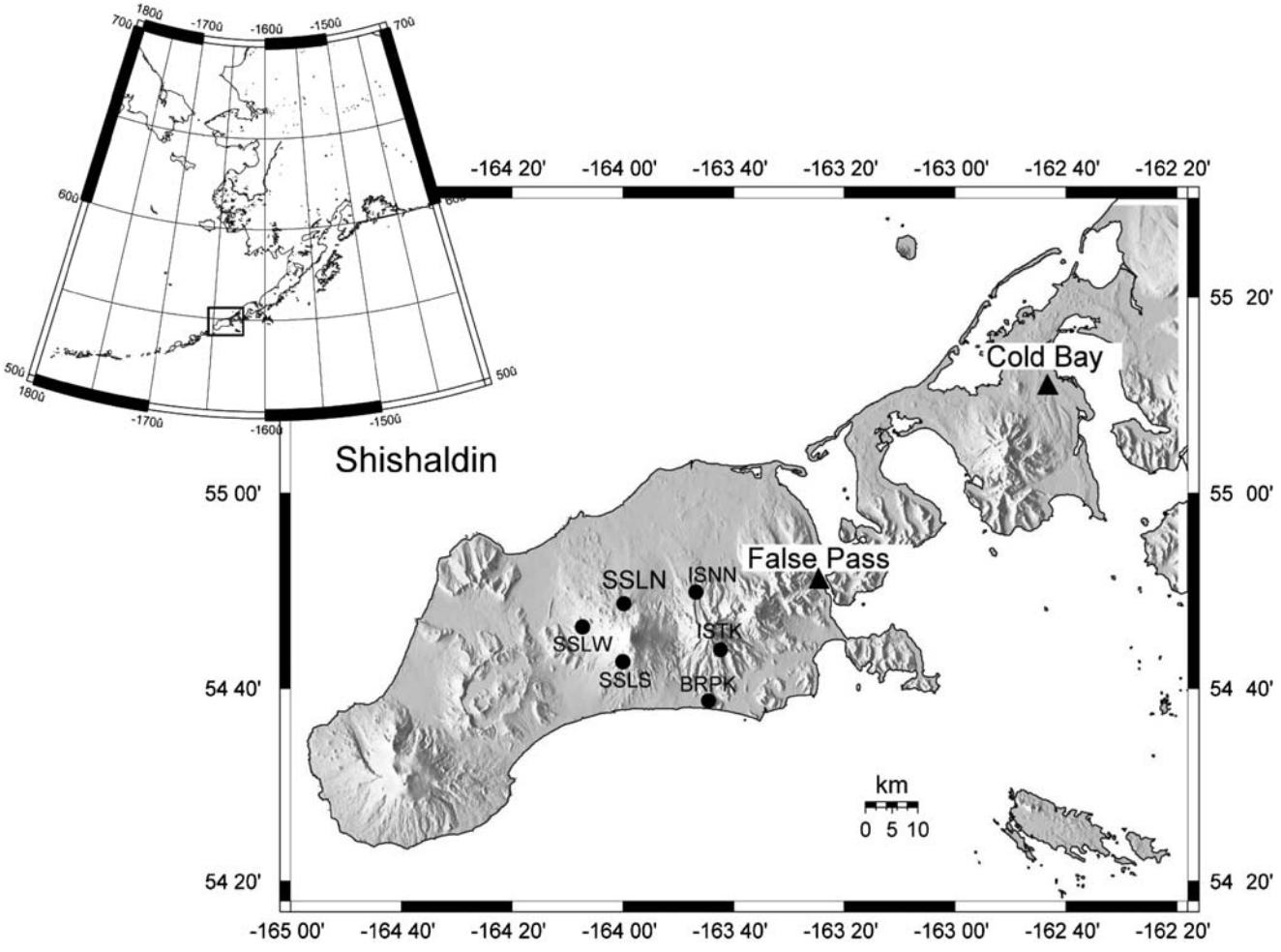

Fig. 1 Map of the Unimak Island and Shishaldin volcano. The black circles mark the locations of the short-period seismometers operated by the Alaska Volcano Observatory (AVO). The pressure sensor used in this study is co-located with seismic station SSLN. The two nearest population centers, False Pass and Cold Bay are also labelled

The 1999 eruption of Shishaldin was preceded by several months of seismic tremor and weeks of thermal anomalies in satellite imagery. On April 18, 1999, AVO researchers performed an overflight of the volcano and acquired infrared imagery of spattering activity with ejection of lava approximately several tens of meters above the vent (Nye et al. 2002). This was the first confirmation of extrusive activity at Shishaldin. The largest phase of eruptive activity began at ≈19h40 on April 19 based on changes in the acoustic and seismic records (Caplan-Auerbach and McNutt 2003). Coincident with this change, satellite images show the development of an ash plume to heights above 16 km. The very sharp increase in tremor intensity on April 7th, correlated with a permanent thermal anomaly above the summit (Nye et al. 2002; Thompson et al. 2002), may mark the openning of the summit vent. Furthermore, the spattering observed 43 hours before the Subplinian phase (Nye et al. 2002), shows that the vent was open at least 30 hours before recording the first hum events of the pre-Subplinian phase.

Data recorded by the pressure sensor on April 19 begin with a prolonged band-limited signal between 2–3 Hz (Caplan-Auerbach and McNutt 2003). Although the signal appears to be continuous, close examination of the waveforms shows that it is composed of discrete pulses of energy, i.e. a close series of hum events (Vergniolle and Caplan-Auerbach 2004). The transition between the pre-Subplinian phase and the Subplinian phase is apparent when the frequency content is displayed with time for both the acoustic and seismic data (Fig. 2). While the spectrum of this "humming signal" remained constant during the ≈13 hours it was recorded, signal amplitude and signal occurrence rate increased with time, with the exception of a brief hiatus thought be associated with two volcanic thermals, discussed later in this paper. The humming signal stopped on April 19 at 19h30 UTC, immediately prior to a major increase in tremor amplitude at 19h35 (Thompson et al. 2002; Caplan-Auerbach and McNutt 2003). The end of the humming signal also coincides with a signal similar to that produced by a Strombolian bubble bursting at a magma surface. This signal, referred to as the "trigger bubble" and described below, is thought to be responsible for the initiation of the Subplinian phase (Vergniolle and Caplan-Auerbach 2004). The Subplinian activity was recorded by the pressure sensor and by the seismic network as a diffuse, ≈47-minute signal with

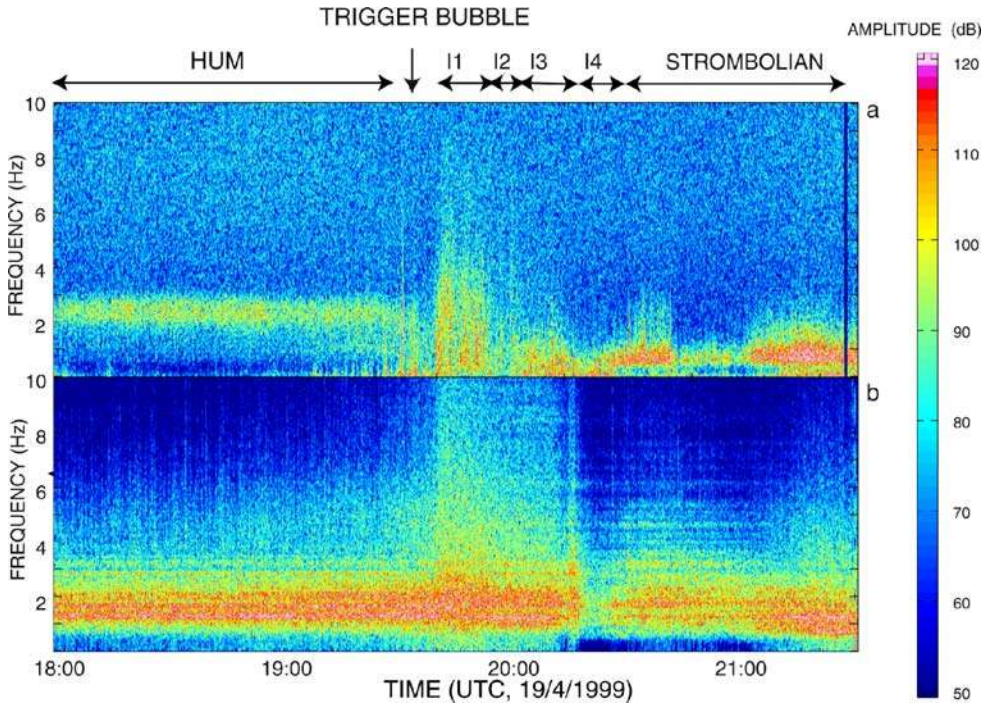

Fig. 2 Frequency as a function of time around the Subplinian phase for **a** acoustic pressure recorded at 6.5 km and **b** seismic signal recorded at 14.8 km from the vent. Spectrograms are calculated on 1024 points (10.24 s) with 80% overlap. The amplitude, in dB, corresponds to the Sound Pressure Level *SPL* for acoustic pressure and to a relative amplitude for the seismic data. *SPL* is equal to $20 \times \log (P_e/P_{ref})$ where P_e is the measured effective rms pressure of the sound wave and P_{ref} the reference effective rms pressure, 2×10^{-5} Pa for airborne sound (Kinsler et al. 1982, Leighton 1994). The time sequence shows the end of the pre-Subplinian phase (hum), an overpressurised bubble representing the transition to Subplinian phase (Trigger bubble), the Subplinian phase with I1 (1st major plume, from 19h40 to 19h55), I2 (1st decompression), I3 (2nd major plume, from 20h04 to 20h17), I4 (2nd decompression) and the first Strombolian phase (from 20h26). Note that there are two gaps of ≈10 s, in each spectrogram, which correspond to calibration pulses, at 21h25 for the pressure sensor and at 20h35 for the seismometer.

energy between 0.5–5 Hz. We note that although it takes ≈19 seconds for signals to propagate from the vent to the microphone, in this paper we simply use the arrival time at the microphone as the event time.

Following the Subplinian phase on April 19, the pressure sensor recorded two periods of signals interpreted as a series of Strombolian bubble bursts, on April 19–20 and April 22–23 (Thompson et al. 2002; Caplan-Auerbach and McNutt 2003). The explosions correspond to a mean bubble radius, length and overpressure, of ≈5 m, ≈12 m and ≈0.083 MPa respectively for the first Strombolian phase and ≈5 m, ≈24 m and ≈0.15 MPa for the second Strombolian phase (Vergniolle et al. 2004). The eruption stopped at the end of May after the production of several additional small ash plumes (Fig. 8 in Nye et al. 2002). The interpretation of the entire eruption chronology, such as the transition between Subplinian and Strombolian activity is discussed in another paper (Vergniolle, subm.).

Gas velocity from acoustic power

Because the source of the sound is sometimes difficult to model, Woulff and McGetchin (1976) have suggested use of acoustic power to estimate gas velocity during volcanic eruptions. In this section, we review the different types of sources and apply this method to the 1999 Shishaldin eruption.

The total acoustic power Π, in Watts, emitted in a half sphere of radius equal to the distance r between the vents and the microphone, here 6.5 km, and radiated during a time interval T, is equal to:

$$\Pi = \frac{\pi r^2}{\rho_{air} c T} \int_0^T |p_{ac} - p_{air}|^2 dt \quad (1)$$

where $\rho_{air} = 0.9$ kg.m^{-3} at 2850 m elevation (Batchelor 1967), $c = 340$ m.s^{-1} is the sound speed (Lighthill 1978) and $p_{ac} - p_{air}$ the acoustic pressure. Acoustic power can thus be easily estimated from acoustic records. However the relationship between acoustic power and gas velocity depends strongly on the source of sound, which can be a monopole, dipole or quadrupole. A monopole source, which radiates isotropically, corresponds to a varying mass flux without external forces or varying stress. For a dipole source, there is a solid boundary which provides an external force on the flow. For a quadrupole source, there is a varying momentum flux which acts on the flow. Explosions, blasts, bubble vibration or balloon bursting are by nature monopole, while a quadrupole source is classically provided by turbulence inside the gas jet. A dipole source is very well adapted to a volcanic gas carrying solid particles (Woulff and McGetchin 1976). In each case, it is possible to calculate acoustic power by assuming that

the signal is periodic and monochromatic with a radian frequency ω.

Monopole source: a tool for the bubble breaking

The source of volcanic explosions has been shown to be a monopole (Vergniolle and Brandeis 1994). For a monopole source, the excess pressure depends on the rate of mass outflow from the source, $\dot{q}$ (Lighthill 1978). If we assume monochromatic oscillations of frequency ω, $\dot{q}$ has the same dimension as ωq. The two are strictly equivalent if oscillations are small. This simplification gives an order of magnitude approximation for acoustic power. Temkin (1981) uses the notation S_ω for the volume flux instead of the mass flux $q = \rho_{\text{air}} S_\omega$ used by Lighthill (1978). For a spherical source of radius R_b,

$$S_\omega = 4\pi R_\text{b}^2 U \tag{2}$$

where U is the radial velocity. By assuming small monochromatic oscillations at frequency ω, acoustic power Π_m radiated in an infinite space is:

$$\Pi_\text{m} = \frac{\rho_{\text{air}} \omega^2 S_\omega^2}{4\pi c} \cdot \tag{3}$$

For small monochromatic oscillations at frequency ω, the oscillatory velocity U has the same dimension as ωR_b (Landau and Lifshitz 1987). Using this approximate value of ω in Eq. (3), acoustic power depends mainly on gas velocity U:

$$\Pi_\text{m} = K_\text{m} \frac{4\pi R_\text{b}^2 \rho_{\text{air}} U^4}{c} \tag{4}$$

where K_m is an empirical constant. $K_\text{m} = 1$ represents the exact solution for a spherical source and $K_\text{m} = 1/16$ is the value to be used for a circular flat orifice (Vergniolle et al. 2004). There is excellent agreement between velocities determined from acoustic power and from bubble breaking models, for both Strombolian bubbles (Vergniolle et al. 2004) and the pre-Subplinian hum events (Vergniolle and Caplan-Auerbach 2004).

Dipole source: a tool for volcanic plumes and thermals

If the source of the sound is due to a steady gas jet containing solid fragments or a gas jet interacting with solid boundaries, the radiation of sound waves is that of a dipole (Woulff and McGetchin1976). A dipole is a set of two monopole sources, oscillating in phase opposition and separated by a distance l, which is small relative to the source-receiver distance. If each of the small source produces a mass outflow $q(t)$ at time t, the excess pressure in the far-field at the distance r is:

$$p_\text{ac} - p_\text{air} = \frac{\cos(\theta) l \ddot{q}(t - r/c)}{4\pi r c} \tag{5}$$

where θ is the angle between the dipole axis and the direction of measurements and c the sound speed (Lighthill 1978). The strength of the dipole $G(t) = l\dot{q}$ is equivalent to an external force acting on the flow. Acoustic power Π_d radiated by such a source in the entire sphere is:

$$\Pi_\text{d} = \frac{l^2 \ddot{q}^2(t - r/c)}{12\pi \rho_{\text{air}} c^3} \cdot \tag{6}$$

As before, if we assume small monochromatic oscillations of frequency ω,

$$\ddot{q}(t) \approx \omega \dot{q}(t) \approx \omega^2 q(t) \cdot \tag{7}$$

For a flat circular source of radius R_mon, the rate of mass outflow $q(t)$ at time t is:

$$q(t) = \rho_{\text{air}} \pi R_\text{mon}^2 U \cdot \tag{8}$$

For small oscillations, the radian frequency ω is equal to the ratio between velocity U and length scale R_mon. Therefore acoustic power Π_d is independent of the exact size of the monopole radius R_mon which is unknown. It can be expressed only as the function of the vertical velocity of the gas jet U as:

$$\Pi_\text{d} = \frac{\rho_{\text{air}} \pi l^2 U^6}{12 c^3} \cdot \tag{9}$$

Our formula is similar to the one calculated by Woulff and McGetchin (1976):

$$\Pi_\text{d} = \frac{K_d \rho_{\text{air}} A_d U^6}{c^3} \tag{10}$$

where A_d is the effective area of the dipole and K_d an empirical constant. Woulff and McGetchin (1976) use a value for K_d of 1.3×10^{-2}, which corresponds to the exact solution of the highly idealised aeolian tone. By using the area of the vent for A_d (Eq. (10)), the calculated gas velocities were twice the values, estimated from a video, of the fumaroles produced by Acatenango volcano (Guatemala), a difference considered by Woulff and McGetchin (1976) to be acceptable. In our calculation, the length of the dipole l corresponds to the average distance between two solid particles, and its maximum value for these longitudinal waves is the diameter of the tube. In that case, our calculation suggests use of a constant K_d of at most of 1/3 in Eq. (10) and less if we use the distance between solid particles in the gas jet. The volume fraction of solid ejecta is rarely estimated

properly during eruptions but, unless the plume is very concentrated in solid particles, the dominant length scale in Eq. (9) is the diameter of the tube. Fortunately, the estimation of gas velocity is only weakly dependant on the empirical coefficient K_d. Note that using a constant $K_d = 1/3$ and the area of the vent in Eq. (10) reconcilies previous observations and calculations on the gas velocity from the fumaroles (Woulff and McGetchin 1976). Therefore in the rest of the paper, we shall use a constant $K_d = 1/3$ and a vent area based on a conduit radius of ≈6 m (Vergniolle et al. 2004), to estimate gas velocity (Eq. (10)). We shall see in the next section how this approach gives very reliable estimates of gas velocity during the pre-Subplinian and the Subplinian phases.

Quadrupole source

A high velocity gas flow in which the gas flux does not vary (no monopole variation) and to which no external forces are applied by the wall (no dipole radiation) will radiate noise as a result of turbulence within the gas jet itself. This is known as aerodynamic noise and it is quadrupole in nature (Lighthill 1978). Turbulence in the jet stream is the main component of jet engine noise. Acoustic power for a quadrupole source is:

$$\Pi_{\mathrm{q}} = \frac{K_q \rho_{\mathrm{air}} \pi R_c^2 U^8}{c^5} \tag{11}$$

where R_c is the conduit radius and K_q an empirical constant, estimated between 3×10^{-5} and 10^{-4} from jet engine noise (Woulff and McGetchin 1976). Quadrupole radiation is much weaker than dipole radiation, which in turn is weaker than monopole radiation. Power laws between acoustic power and velocities, which are calculated by assuming small pressure oscillations, break down if the flow is supersonic.

Description of the Subplinian phase

The Subplinian phase was recorded on both the acoustic and seismic sensors as a 46-minute signal with frequencies strongest between 0–5 Hz (Fig. 2). The signal fluctuates in intensity: in some sections between 19h40 and 20h26, both acoustic and seismic signals are strong while in other sections one or both of the signals weakens (Fig. 2). At 20h26, the first Strombolian phase starts, as denoted by the first explosion signal recorded by the pressure sensor since the beginning of the Subplinian phase (Fig. 2). However, if we look in detail at the acoustic record, there are two low frequency bursts, one close to the trigger bubble at 19h31 and one several minutes later at ≈19h34, which are not evident in the seismic data (Fig. 2). Pilots flying over the volcano at the time report that the Subplinian plume was formed by two successive jets, the second one higher than the first. No precise measurements were performed, but observations suggest heights of 9 km and 16 km (Stelling et al. 2002). Here we suggest that the first jet occurs around the trigger bubble whereas the second one is marked by strong acoustic and seismic signals and initiates near 19h40.

Gas velocity estimates from acoustic power

Although the acoustic waveform recorded during the Subplinian phase is rather complicated, the use of acoustic power allows us to place constraints on gas velocity (Fig. 3). The sound emitted by a steady gas jet carrying solid fragments has been shown to be a dipole source. Using a coefficient of $K_{\mathrm{d}} = 1/3$, Eq. (10) gives an lower bound on the gas velocity.

In our calculations we assume that all of the signal recorded by the pressure sensor has come from Shishaldin itself and the influence of other signals such as wind is not considered. There are no meteorological stations near the pressure sensor, so the wind strength at the time of the eruption is unknown. It is therefore possible that our values for gas velocity are overestimated due the presence of acoustic signals resulting from wind. However, seismic data at the time do not show the broadband signal characteristic of high winds at the site. Furthermore the sensor was set north to the volcano, in a location protected from the prevailing winds, as marked by the ash deposits south of the volcano (Fig. 2 in Stelling et al. 2002).

We first consider the gas velocity during the Subplinian phase (Fig. 3). A first look at temporal changes in gas velocity shows that the Subplinian phase may be divided into two discrete time periods, from 19h40 to 19h55 and from 20h10 to 20h17. These two phases were originally noted by Caplan-Auerbach and McNutt (2003) based on the spectral content of both the seismic and acoustic data (Fig. 2). These periods are defined by a rapid increase in gas velocity followed by a roughly linear decrease in gas velocity. A good example of constant decrease starts at ≈19h40 mn (Fig. 3) for a duration of ≈331 s, corresponding exactly to the start of the strong tremor recorded at all of the seismic stations (Fig. 2). However, the period between the trigger bubble, at ≈19h31, and the strong tremor, at ≈19h40, has a very similar trend in gas velocity to that of the period after 19h40 (Fig. 3). Furthermore, acoustic pressure also displays two bursts of low-frequency energy during that period, which are very similar to those occurring between 19h40 and 19h55, albeit with a smaller intensity (Fig. 2). Therefore, we propose that the period between 19h31 and 19h40 is in fact part of the Subplinian phase.

In Fig. 3, we recognize six periods of roughly linear decrease in gas velocity with time, each separated by a period of roughly constant increase. The decrease in gas velocity with time has approximately the same slope for the six periods (Fig. 3), suggesting that the same mechanism is at work within the conduit (Table 1). The duration of the gas velocity periods ranges from ≈80 s for the first period to ≈309 ± 105 s for the remaining five periods (Table 1).

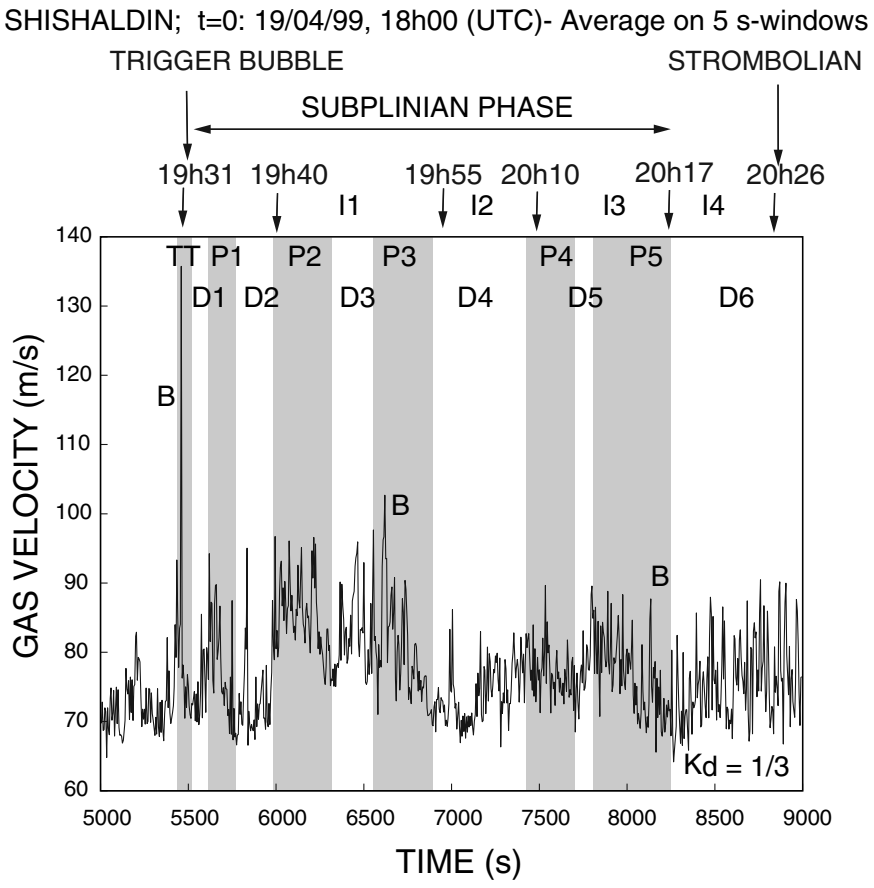

Fig. 3 Gas velocity (m/s) estimated from acoustic power and using aconstant of $K_d = 1/3$, a vent area based on a conduit radius of ≈6 m (Vergniolle et al. 2004) and a dipolar source (Eq. (10)). Gas velocity is calculated over a time window of 5 s without any overlapping between windows.Acoustic data were filtered above 0.01 Hz to remove the signal related to long term variations in atmospheric pressure. This also has the effect of partly removing the contribution of the wind, which is strongest in the lowest frequency part of the spectra. Note that the approximation of a dipole source is not valid outside of the Subplinian phase and produces an overestimateof the gas velocity by a factor of ≈3.3 for the trigger bubble and any other bubbles, named B. Note that six periods can be described, TT is the trigger thermal and P1 to P5 the five later plumes. D1 to D6 corresponds to the six decompression periods.

Between each velocity decrease there is a time period in which velocity increases again (Fig. 3). We propose that these six periods of velocity decrease correspond to the emission of six "plumes," in which the motion of the magmatic mixture is upwards (Fig. 3) and that the Subplinian activity is actually the result of these six events. We further suggest that the intervals in which gas velocity increases correspond to a "decompression" phase. This decompression phase occurs when residual gas in the conduit expands due to the removal of the weight of the previous plume, leading to the next plume (Vergniolle and Caplan-Auerbach, subm.). Later we will consider whether

Table 1 Estimates for the trigger thermal (0) and the five "plumes" (1 to 5) observed during the Subplinian phase. Time equal 0 refers to 18h00 and real time are respectively19h30mn40s, 19h33mn35s, 19h39mn43, 19h49mn13s, 20h3mn44s, 20h10mn4s. Gas velocity is calculated by using Eq. (10) with a constant K_d of 1/3 and a vent area based on a conduit radius of ≈6 m (Vergniolle et al. 2004). Mean is the mean value for the five "plumes" or "decompressions" (decomp.) without the trigger thermal, as it will be shown to have a different origin than the rest of the five plumes (Vergniolle and Caplan-Auerbach, subm.). Std means standard deviation, Vol means volume and Vel means measured velocity. Aver means average, Max maximum and Min minimum. Slope is the decrease of measured gas velocity in time. Decompression time of plume 1 is the time between plume 1 and 2, and right after plume 1. Gas volume used for calculating gas flux is the gas volume expelled during the trigger thermal (0) and the five "plumes" (1 to 5). Gas flux is based on the total duration of the six "plumes" (0 to 5) and the six "decompression periods.

Plume	0th	1st	2nd	3rd	4th	5th	Mean	Std	Tot
Initial Time (s)	5440	5615	5983	6553	7424	7804			
Duration (s)	80	157	332	337	274	445	309	105	2806
Aver. Vel ($m.s^{-1}$)	83	82	86	84	78	80	82	3.2	
Max. Vel ($m.s^{-1}$)	94	94	95	97	83	90	92	5.7	
Min. Vel ($m.s^{-1}$)	73	70	77	72	74	71	73	3.0	
Slope ($\times 10^{-2}$ $m.s^{-2}$)	26	1.5	5.4	7.6	3.3	4.0	7.2	4.8	
Gas Vol ($\times 10^6$ m^3)	0.76	1.5	3.3	5.2	2.4	4.0	2.5	1.2	15.1
Gas Flux ($\times 10^3$ m^3/s)	9.4	9.3	9.8	9.6	8.9	9.1	9.3	3.3	4.5
Decompression	0th	1st	2nd	3rd	4th	5th	Mean	Std	Tot
Duration (s)	94	211	238	534	103	534	324	198	1715

these time periods are associated with significant gas release and whether they should be included in gas volume calculations.

Note that these decompression phases are similar to the period immediately preceding the first Strombolian phase (between 20h17 and 20h26) in terms of both duration (324 ± 198 s) and evolution of gas velocity. This suggests that the first Strombolian phase, with its rapid sequence of large bubbles breaking at the vent, may also result from the decompression induced by the sudden removal of gas and magma from the conduit during the Subplinian phase.

The period following the first velocity decrease is very short, ≈94 s, compared to the average duration between the rest of the plumes (Table 1). This fact, combined with the short duration of the first period, encourages us to label this first phase as a "thermal," i.e. an instantaneous rather than prolonged release of gas (Turner 1973; Sparks et al. 1997).

Note also that the beginning of each period is defined by the local maximum in gas velocity. Since the gas velocity is calculated with a time averaging of 5 s, there is an uncertainty of ±5 s, on both sides of the signal. Because the end of each period is determined with less precision than the beginning, we estimate an uncertainty of 20 s in the durations. This only leads to a ±2% error in gas volume and gas flux. If the conduit radius is twice the value determined from acoustic measurements (Vergniolle et al. 2004), the gas velocity is reduced by 25%, with a comparable change in gas flux and volume. Given the uncertainty associated with wind noise and the constant $K_d = 1/3$, our determination of gas volume and gas flux is probably within 30% accuracy.

Validation of the acoustic power method

An important result from our calculation of gas velocity is that it always lies below the sound speed, making the use of the acoustic power technique valid. Secondly we note that the assumption of a dipolar source of sound has been made for the whole time sequence in Fig. 3. If any monopolar explosions occur during that time, the dipole assumption results in a dramatic overestimate of gas velocity, by roughly a factor of 3.3. This is the case for the trigger bubble, which shows a velocity of ≈140 m/s instead of 70 m/s and for the several large overpressurised bubbles occurring later in the record which are detected by their waveforms (Fig. 3). For a quadrupole source, i.e. produced by turbulence in the gas jet free of solid fragments, the velocity will be underestimated by a dipole approximation. This might be the case for the sound produced between the end of the Subplinian and the start of the Strombolian phase and during the decompression periods (Table 1). However at these times, strong variations in magma column height are very likely as the bubbly magma expands under the pressure release resulting from the expulsion of a large volume of gas and magma. In that case, the sound produced will be that of a monopole source, the strong acoustic radiation of which can totally mask any dipole or quadrupole source (Woulff and McGetchin 1976). Therefore, the velocity of the decompression periods may be overestimated by a factor of 1.9, giving an average velocity of less than 40 m/s (Fig. 3).

Our results show that gas velocity during the Subplinian phase is large, ≈82±3.2 m/s (Fig. 3). This value is slightly lower than velocities found for other large explosive basaltic eruptions: Williams (1983) estimates muzzle velocities of 150 m/s and 170 m/s for two basaltic Plinian eruptions of Masaya volcano, and Walker et al. (1984) state that the muzzle velocity for the 1886 Tarawera eruption exceeded 250 m/s. The velocity during the Shishaldin Subplinian phase, ≈82 m/s, is very similar to the velocity estimated from ballistics between 40 and 180 m/s during the Vulcanian explosions and the Subplinian column of andesite at Soufrière Hills (Montserrat Island, West Indies) (Druitt et al. 2002). Durations are also very similar, with ≈48 minutes at Soufrière Hills (Robertson et al. 1998; Druitt et al. 2002).

Plinian columns are often marginally stable and can collapse to produce pyroclastic flows when the mixture becomes too heavy for vertical motion (Carey et al. 1990; Sparks et al. 1997; Kaminski and Jaupart 2001). Therefore the possibility exists that the "decompression" phases observed between "plumes" at Shishaldin volcano are associated with the collapse of a buoyant plume into a heavy pyroclastic flow. However no evidence of pyroclastic flows was found either in satellite imagery taken during the eruption, in field deposits or recognised on seismic records (Dehn et al. 2002; Stelling et al. 2002; Thompson et al. 2002), so another mechanism must be invoked.

Spectral content of the Subplinian phase

We calculated fast Fourier transforms on acoustic pressure filtered above 100 s for each of the periods defined by trends in gas velocity (Fig. 3). The Subplinian phase appears as a broadband event, with a spectral maximum decreasing from ≈2 Hz at the time of the trigger thermal (Fig. 4b) to ≈0.8 Hz for the last plume P5 (Fig. 4g). The constant frequency of the hum (Vergniolle and Caplan-Auerbach 2004) is very clear on the fast Fourier transform calculated before the Subplinian phase (Fig. 4a).The frequency content of the first five decompression phases has no characteristic frequency, in contrast to the last decompression (Fig. 4g), which shows a well marked peak at ≈0.8 Hz. The progressive appearance of the ≈0.8 Hz peak into the spectrum is related to the increasing number of large bubbles breaking at the top of the magma column as the eruption approaches the first Strombolian phase.

To further examine the six periods considered to be plumes or thermals, we filtered the acoustic record in narrow frequency bands and calculated the maximum signal amplitude in each band (Fig. 5). The start of each of the six periods, previously defined by jumps in gas velocity (Fig. 3), appears as a sharp increase in amplitude in either the low-frequency band, from 0.01 Hz to 0.5 Hz, or in the middle band, between 0.1 and 1 Hz (Fig. 5). In contrast to

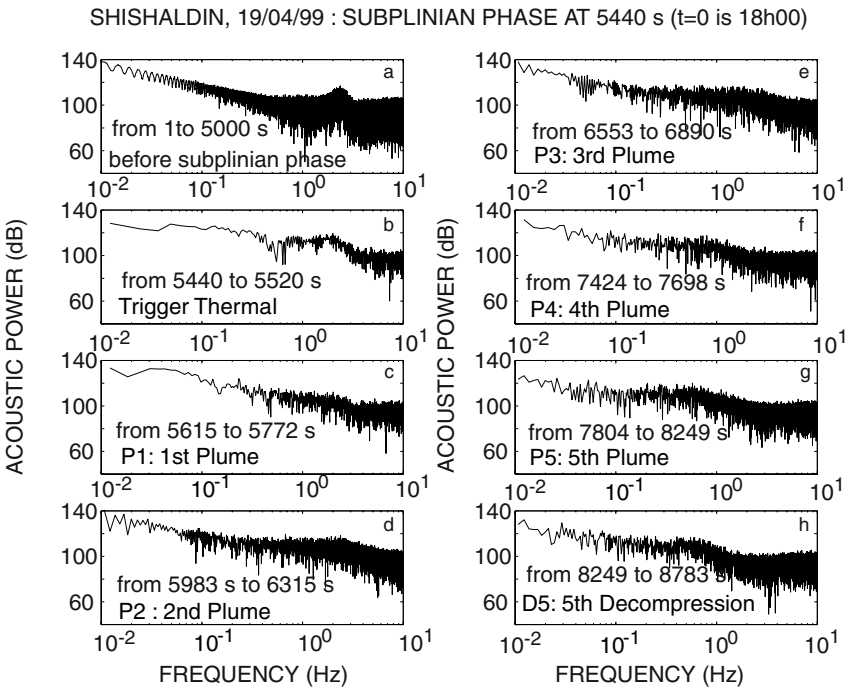

Fig. 4 Fast Fourier Transform calculated on acoustic pressure-filtered above 100 s in decibels (see caption in Fig. 2) and for each of the period defined by the gas velocity. Note that the time periods noted in each panel are in seconds relative to 18h00 UTC **a** before the Subplinian activity (from 1 s to 5000 s), **b** for Trigger thermal (from 5440 s to 5520 s), **c** for the first plume P1 (from 5615 s to 5772 s), **d** for the second plume P2 (from 5983 s to 6315 s), **e** for the third plume P3 (from 6553 s to 6890 s), **f** for the fourth plume P4 (from 7424 s to 7698 s), **g** for the fifth plume P5 (from 7804 s to 8249 s), **h** for the last decompression, D5, before the second Strombolian phase (from 8249 s to 8783 s). The Subplinian phase appears as a broadband frequency event, with a migration of the maximum from ≈2 Hz in the trigger thermal (b) to ≈0.8 Hz in the last plume P5 (g).

the low frequency range (Fig. 5a), the intensity of the hum events, as shown by the 0.5 Hz–4 Hz range, does not show any change for the couple of hours prior to the Subplinian phase (Fig. 5b). The start of the first Strombolian phase is very clear in the 0.5–4 Hz range, as explosions have peaks between 0.7 and 0.8 Hz (Vergniolle et al. 2004) gradually increasing in strength (Fig. 5b).

Initiation of a basaltic Subplinian phase

We propose that the Subplinian phase observed at Shishaldin is the result of the sudden collapse of a foam of ≈2.0 km trapped within the volcanic conduit (Eq. (10) in Vergniolle and Caplan-Auerbach, subm.). Because the trigger bubble is formed at the depth of the reservoir (Vergniolle and Caplan-Auerbach 2004), its rise through a bubbly magma column might be responsible for shaking the magma column strongly enough to instigate its collapse. We explore this possibility below.

Transition between the pre-Subplinian and Subplinian phase

At 19h31 mn, the pre-Subplinian phase ends and the acoustic pressure changes from the constant ≈2 Hz frequency humming phase to a waveform characteristic of a Strombolian bubble breaking (Vergniolle et al. 2004; Vergniolle and Caplan-Auerbach 2004). The waveform for this event is characteristic of the sound produced by the strong vibration of a large overpressurised bubble which breaks at the top of the magma column (Vergniolle and Brandeis 1994, 1996). Modelling the bubble vibration leads to estimates on bubble radius, length and overpressure of 5 m, 15 m and 0.42 MPa respectively (Vergniolle et al. 2004; Vergniolle and Caplan-Auerbach 2004). Its large overpressure, above the "normal" value of ≈0.083 MPa and ≈0.15 MPa during the two Strombolian phases, suggests that this bubble is formed at the depth of the reservoir (Vergniolle 1998; Vergniolle and Caplan-Auerbach 2004). Although the internal gas overpressure is rather large, the acoustic signature of the trigger bubble cannot be detected on the seismic network. It is related to both a strong tremor at the time and to the preferential expansion of the large bubble towards air rather than ground. This observation will have consequences on the monitoring of basaltic plumes eruptions, such as at Shishaldin.

The acoustic pressure record (Fig. 6) shows two pulses prior to the trigger bubble. The first one (at 5324 s, Fig. 6a) has a frequency of ≈0.7 Hz, similar to that produced by Strombolian explosions. The best fit between observed (Fig. 6a) and synthetic waveforms (Vergniolle et al. 2004) is obtained for a bubble of ≈3.5 m in radius, ≈20 m in length and with a gas overpressure of ≈0.13 MPa. Note that this value is smaller than that of the trigger bubble. The second pulse (at 5382 s, Fig. 6b) has a frequency and an amplitude (≈2 Hz and ≈1.5 Pa respectively)

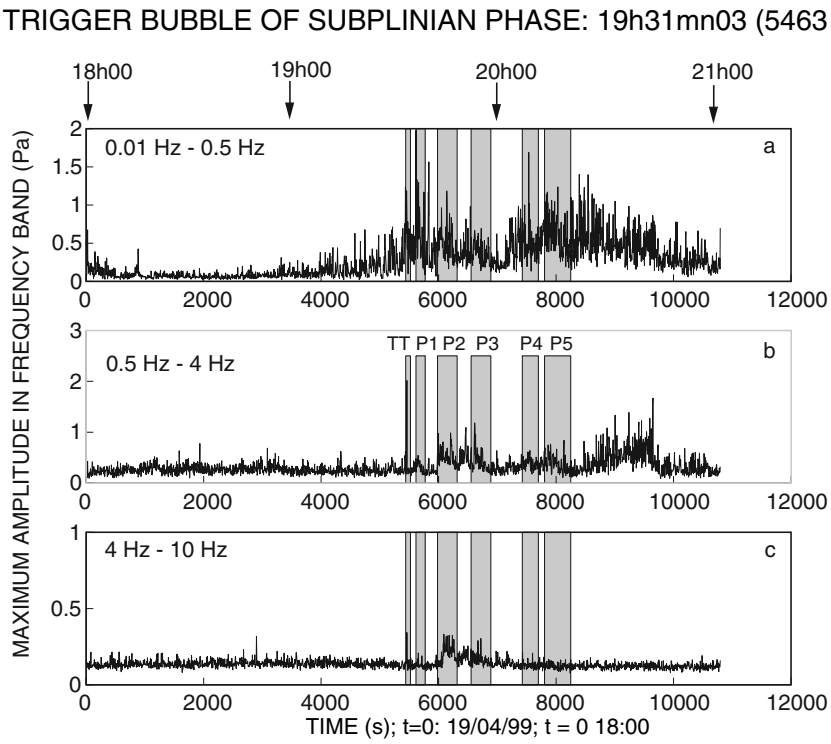

Fig. 5 The maximum amplitude of acoustic pressure (Pa) in three frequency bands is followed in time, from 18h00 to 21h00 the 19th of April 1999. Each of the periods, previously defined by jumps in gas velocity (grey shadding), are marked by a sharp increase in amplitude, either in the low frequency range, from 0.01 Hz to 0.5 Hz, for the trigger thermal and plumes P1, P3, P5 or in the middle range for plumes P2 and P4 **a** In the low frequency, from 0.01 Hz to 0.5 Hz, there is a regular increase in intensity ≈1463 s (at ≈4000 s) prior to the trigger bubble (at 5463 s), possibly indicative of the bubble rise in the conduit. **b** There is no change in the intensity of hum events prior to the Subplinian phase in the middle range, from 0.5 Hz to 4 Hz. The start of the first Strombolian phase is very clearly marked as the explosions, ≈0.8 Hz, gained strength. **c** Only the trigger bubble and the second plume P2 has some energy in the "high" frequency range, from 4 Hz to 10 Hz.

ressembling those produced by the hum events. In that case, the bubble length and overpressure are 76 m and $\approx 9.5 \times 10^{-3}$ MPa respectively, when using the hum synthetic waveforms (Vergniolle and Caplan-Auerbach 2004). However, the trigger bubble with its large overpressure is the major event occurring at the beginning of the Subplinian phase.

Since the beginning of the Subplinian phase has been placed at $\approx 5440 \pm 5$ s (Fig. 3), the second strongest pulse at ≈5435 s may mark the exact start of the Subplinian phase (Fig. 6c). This pulse, however, cannot be modelled by the vibration of a large overpressurised bubble as for the trigger bubble. Hence it probably corresponds to the rupture of the foam, which may have occurred ≈28 seconds before the actual breaking of the trigger bubble at the surface.

The trigger bubble

If we define the beginning of the subplinian phase by changes in gas velocity (Fig. 3), the initiation of the Subplinian eruption starts just before the arrival of the trigger bubble at the surface. However, the formation of the trigger bubble at the depth of the reservoir occurs well before it arrives at the surface (Figs. 7 and 8). The upwards velocity U_b of a large bubble almost as large as the conduit and rising in a tube full of stagnant liquid depends mainly on the radius of the tube R_c and not on the bubble length (Wallis 1969):

$$U_b = 0.345\sqrt{2gR_c} \cdot \tag{12}$$

Equation (12) results from a balance between inertia and buoyancy, in which gas density is negligible compared to liquid density. Hence, the slug velocity is independant of the mixture density.

The conduit radius R_c can be estimated from the initial bubble radius R_o and from the thickness δ of the magma present between the bubble and the solid wall, called the lateral film. If we assume that the thickness δ has reached its asymptotic value δ_∞, it can be calculated as (Batchelor 1967):

$$\delta_\infty = 0.9R_c \left(\frac{\mu^2}{\rho^2 R_c^3 g}\right)^{1/6} \tag{13}$$

where μ and ρ are respectively the viscosity and the density of the mixture, R_c the conduit radius, assumed at first order to be the bubble radius R_o and g the acceleration of gravity. For a magma viscosity of 500 Pas, and a bubble radius of 5 m (Vergniolle et al. 2004), the vertical film δ_∞

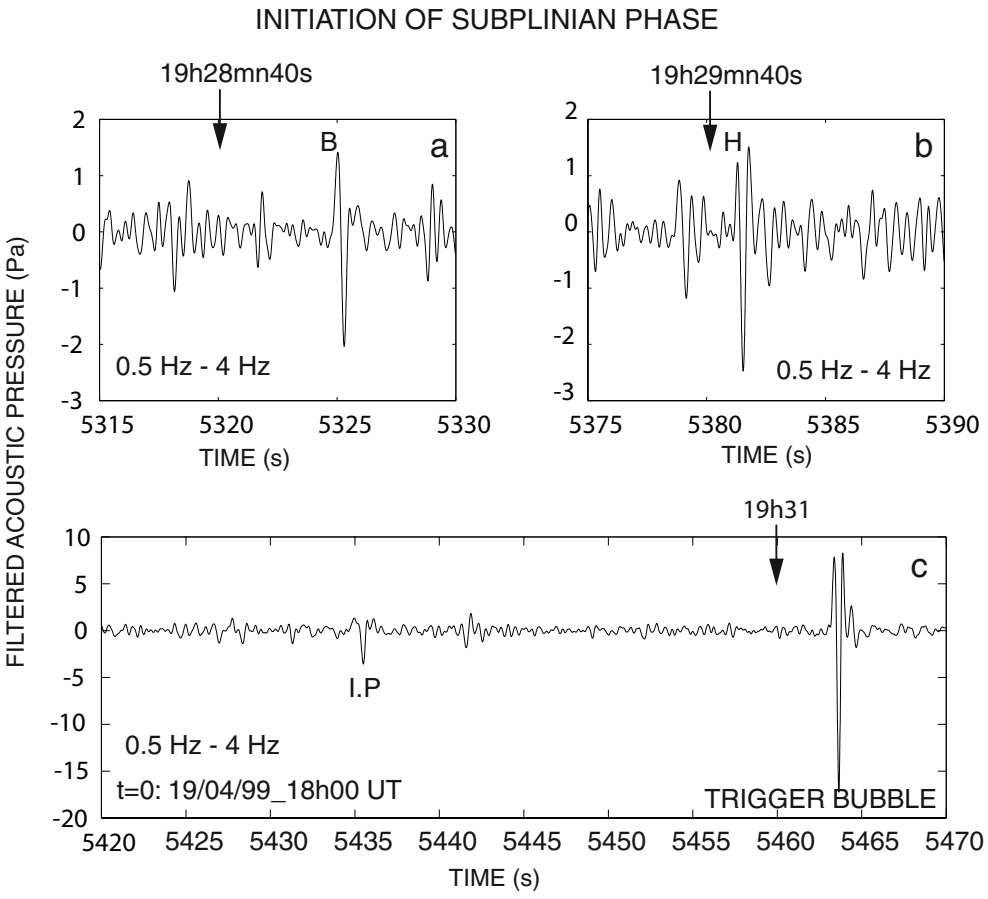

Fig. 6 Acoustic waveforms at the transition between the pre-Subplinian phase and the start of the Subplinian phase at t = ≈5440 ± 5 s, for an initial time taken at 18h00 (Fig. 3). Data are filtered between 0.5 Hz and 4 Hz with a two-way filter to keep a zero phase lag, hence an exact time. This filtering allows a much better determination of the physical process, such as bubble breaking. **a** B is a bubble, whose frequency ≈0.7 Hz corresponds to a radius, length and overpressure of 3.5 m, ≈20 m, ≈0.13 MPa respectively. **b** H marks where a hum event is seen on acoustic pressure, corresponding to a radius, length and overpressure of 3.5 m, 76 m, $\approx 9.5 \times 10^{-3}$ MPa. **c** waveform of the trigger bubble preceded by a relatively strong pulse 28 s beforehand (I P: initial pulse), which may mark the initiation of the foam rupture in the conduit.

around each bubble is ≈0.86 m. Because the asymptotic value δ_∞ is seldom attained even for long bubbles (Fabre and Linné 1992) and corresponds to a minimum value, the conduit radius can be safely estimated at ≈6 m from acoustic measurements.

However if the overlying mixture is a foam, its density ρ and viscosity μ are the one of the foam, ρ_{foam} and μ_{foam} respectively:

$$\rho_{\text{foam}} = \epsilon\, \rho_{\text{gas}} + (1 - \epsilon)\, \rho_{\text{liq}} \tag{14}$$

where ϵ are is the gas volume fraction. The large density difference between liquid and gas makes:

$$\rho_{\text{foam}} \approx (1 - \epsilon)\rho_{\text{liq}} \tag{15}$$

a very good approximation. We also assume that the gas volume fraction is constant with depth in the overlying foam and equal 0.6 (Vergniolle and Caplan-Auerbach, subm.). The foam viscosity μ_{foam} depends on the liquid viscosity μ_{liq} by (Jaupart and Vergniolle 1989; Vergniolle et al. 2004):

$$\mu_{\text{foam}} = \frac{\mu_{\text{liq}}}{(1 - \epsilon)^{5/2}}\,. \tag{16}$$

Once the trigger bubble enters the foam, the vertical film around it becomes 2.5 m (Eq. (13)).

Note that previous synthetic waveforms of the trigger bubble and of the hum events have assumed that the large bubbles were rising in a pure liquid (Vergniolle and Caplan-Auerbach 2004). Therefore the bubble radius was taken to be ≈5 m as for a pure magma, whereas it should have been taken to be ≈3.5 m for a conduit radius of ≈6 m and for a foam (Vergniolle et al. 2004). The synthetic waveform (Vergniolle et al. 2004) of the trigger bubble of the Subplinian phase was redone and gave an excellent fit with the data, with a bubble length of ≈35 m and a gas overpressure of ≈0.39 MPa. Because the synthetic waveforms of the hum events are those of a linear oscillator (Vergniolle and Caplan-Auerbach 2004), a decrease in bubble radius and in the hole radius only increases the bubble length, to ≈86 m, and decreases the gas overpressure to a value from $\approx 0.84 \times 10^{-3}$ MPa to $\approx 3.2 \times 10^{-3}$ MPa.

The bubble rise velocity should also include a correction factor if the fluid is viscous, giving a bubble velocity of:

$$U_{\text{b}} = 0.345\sqrt{2\text{g}\text{R}_{\text{c}}}\left[1 - \exp\left(\frac{-0.01\, N_{\text{f}}}{0.345}\right)\right] \tag{17}$$

where:

$$N_{\text{f}} = \frac{\rho\sqrt{8\text{g}\text{R}_{\text{c}}^3}}{\mu}\,. \tag{18}$$

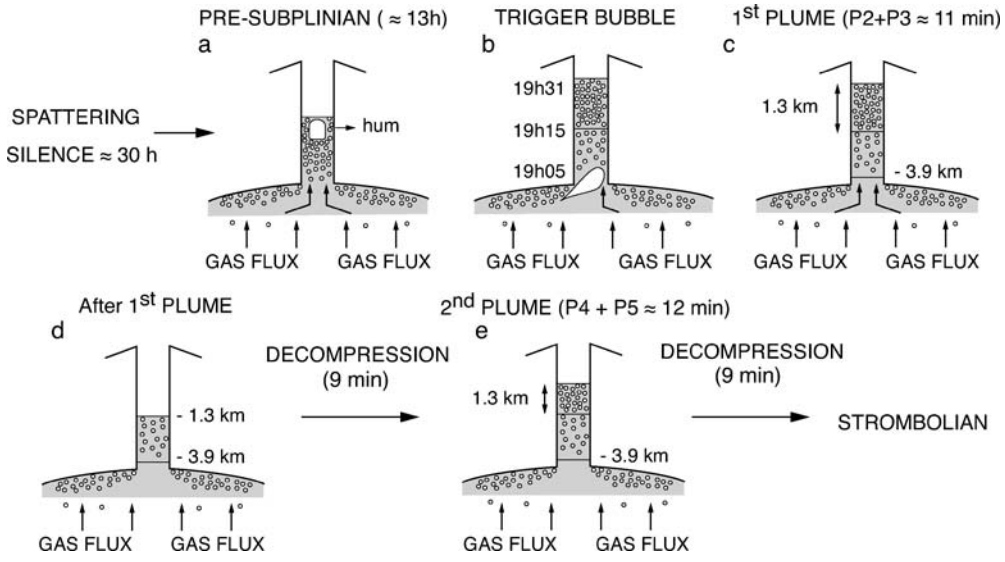

Fig. 7 Sketch of the various eruption regimes around the Subplinian phase, for the simplified case of only two plumes (see text for details). **a** Pre-Subplinian phase, characterised by "hum" events corresponding to the local coalescence within the foam in the conduit. **b** Trigger bubble is a large overpressurised bubble which starts rising in the conduit, ≈26 minutes before breaking. It enters the foam ≈16 minutes before breaking and shakes the foam until it collapses entirely, ≈28 seconds before the trigger bubble breaks at the surface. **c** First plume of the Subplinian phase (P2 and P3): entire collapse of a foam of ≈1.3 km length (Eq. (10) in Vergniolle and Caplan-Auerbach, subm.). **d** Decompression induced by the sudden withdrawal of magma and gas in the conduit. **e** Second plume of the Subplinian phase (P4 and P5): entire collapse of a foam of ≈1.3 km length (Eq. 10 in Vergniolle and Caplan-Auerbach, subm.) followed by 9 minutes of decompression before starting the first Strombolian phase

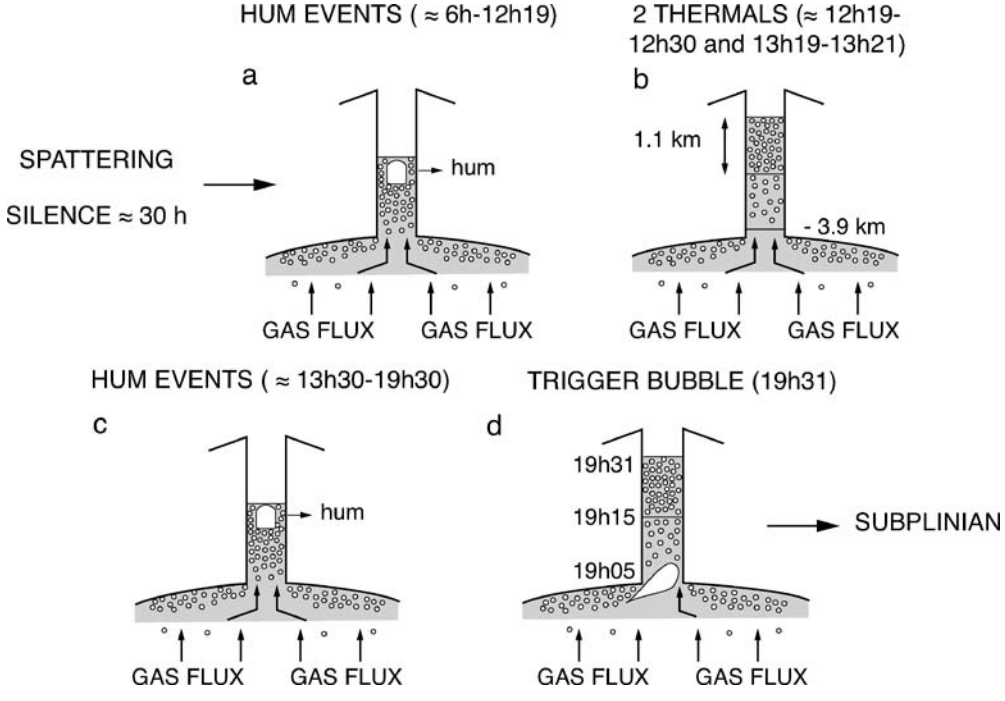

Fig. 8 Sketch of the various eruption regimes in the pre-Subplinian phase **a** Pre-Subplinian phase, from 6h00 to 12h19, characterised by "hum" events corresponding to local coalescence within afoam building up in the conduit. **b** Formation of two thermals between 12h19–12h30 and13h12–13h21, reaching a maximum height of 3 km in the atmosphere. Each thermal phase corresponds to a foam of ≈1.1 km in length (Eq. 10 in Vergniolle and Caplan-Auerbach, subm.). **c** Pre-Subplinian phase, from 13h30 to 19h30: hum events resume. **d** Trigger bubble, at 19h31, is a large overpressurised bubble which starts rising in the conduit, ≈26 minutes before breaking (Fig. 5). It enters the foam ≈16 minutes before breaking and shakes the foam until the completecollapse occurs just before the trigger bubble breaks at the surface (Vergniolle and Caplan-Auerbach, subm.)

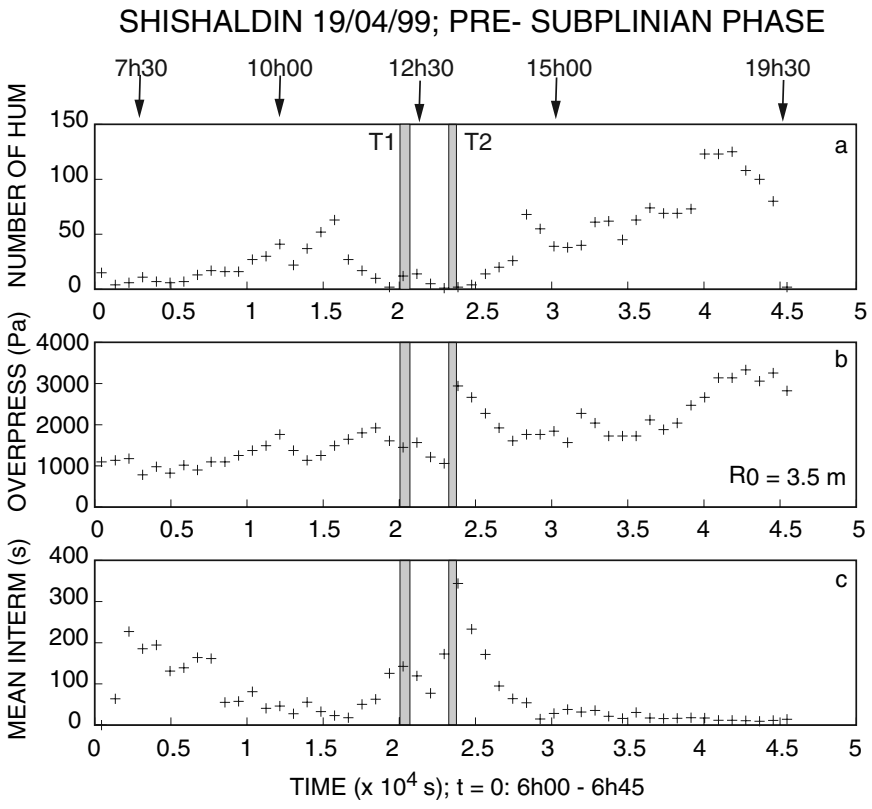

Fig. 9 Hum events of the pre-Subplinian phase, detected with a coherence threshold of 0.7, are stacked over 15 minutes starting at 6h00. Note that the first value is averaged over 45 minutes due to the low number of hum events. **a** number of events, **b** average gas overpressure (Pa) when using a bubble and hole radius of ≈3.5 m as for rising in a foam, **c** average intermittency between 2 hum events (s). The grey domains correspond to the two thermal phases, T1 from 12h19 to 12h30 and T2 from 13h12 to 13h21

The trigger bubble rises in a tube of radius ≈6 m, through a magma of viscosity $\mu_{liq} = 500$ Pa.s, at a velocity U_b of ≈3.7 m/s when ignoring viscous effects (Eq. (12)). However, when the trigger bubble enters the foam, the apparent viscosity of the fluid increases (Eq. (16)) and its density decreases to 1080 kg.m^{-3} (Eq. (15)), giving a velocity of ≈2.1 m/s (Eq. (17)). Thus there is a period of ≈16 minutes, based on a 2 km-long foam (Vergniolle and Caplan-Auerbach, subm.), during which the trigger bubble rises through the conduit. During that time, the bubble rise disturbs the foam before breaking at the surface. However the acoustic pressure, recorded 16 minutes before the trigger bubble, shows neither a sharp increase in the number of hum events nor a sharp increase in their intensity (Vergniolle and Caplan-Auerbach 2004). Therefore there is no evidence at the surface that the trigger bubble, while rising, induced more local coalescence in the uppermost part of the foam trapped in the conduit (Fig. 5b; Fig. 9).

If the foam rupture starts at ≈5440±5 s and propagates downwards with a velocity of 5.6 m/s (Vergniolle and Caplan-Auerbach, subm.), the initial position of the trigger bubble at that time (≈5440±5 s) is ≈220 m below the top of the magma column, as the upwards motion of the bubble, ≈2.1 m/s, is combined with the downwards motion of the rupture front, ≈5.6 m/s (Vergniolle and Caplan-Auerbach, subm.). Because the conduit radius is ≈6 m (Vergniolle et al. 2004), the trigger bubble is at a depth of ≈18 times the conduit diameter when the trigger thermal starts. Hence we suggest that the initiation of the Subplinian phase may be related to the approach of the trigger bubble close to the top of the foam. The physics of such an initiation, being complex, is beyond the scope of the present study and will be left for for future work.

Examination of the low-frequency acoustic signal (0.01 Hz to 0.5 Hz) shows a regular increase in intensity beginning ≈1463 s before the trigger bubble (Fig. 5a) and ending with the start of the Subplinian phase. Because the formation of the trigger bubble at depth is probably violent, as suggested from its large overpressure (Vergniolle 1998; 2001), once the bubble enters the conduit, its strong expansion may induce motions at the top of the magma column. Gravity waves are likely to be formed at the magma surface with fundamental frequencies at ≈0.3 Hz and ≈0.4 Hz for a conduit radius of 6 m and, respectively, the angular and radial modes (Vergniolle et al. 1996). Therefore we suggest that the increase seen at ≈4000 s in the 0.01 Hz–0.5 Hz range may mark the injection of the trigger bubble at the base of the conduit. This corresponds to a depth of ≈3.9 km for a foam of ≈2.0 km. Although no independant constraint exists on the magma chamber depth below Shishaldin, thevery good agreement with other basaltic reservoirs, such as Kilauea (Hawaii) and Etna (Klein 1987; Ryan 1988; Laigle and Hirn 1999; Laigle et al. 2000; Schmincke 2004) is in favor of this interpretation.

Two thermal phases in the middle of the pre-Subplinian phase?

The long series of hum events of the pre-Subplinian phase have been stacked and modelled to find the

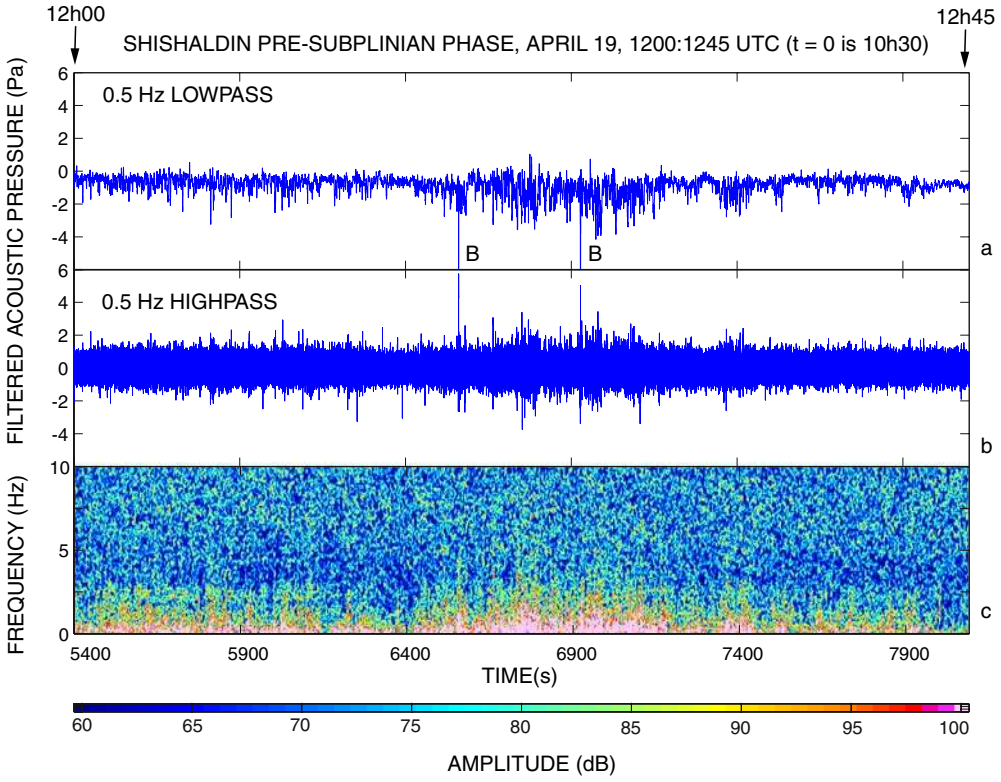

Fig. 10 Acoustic pressure (Pa) as a function of time (s) around the first thermal phase at 12h19. **a** filtered below 0.5 Hz and **b** above 0.5 Hz. B marks the position of a few large bubbles. **c** Spectrogram of acoustic pressure, calculated on 1024 points (10.24 s) with 80% overlap and a sampling frequencyof ≈100 Hz. The amplitude in dB is calculated as in Fig. 2) and using a reference rms pressure equal to 20 μPa (Kinsler et al. 1982, Leighton 1994)

characteristics of the source (Vergniolle and Caplan-Auerbach 2004). This "humming signal" is interpreted as a local coalescence within a long foam building up in the conduit, which produces large gas bubbles, ≈86 m in length, before bursting (Fig. 8). The gas overpressure is small, from 0.84×10^{-3} MPa to 3.2×10^{-3} MPa and is related to the bubble capillary pressure inside of the foam (Vergniolle and Caplan-Auerbach 2004). The top of the foam is composed of bubbles with diameters from ≈1.9 mm at the beginning of the episode towards ≈0.5 mm at its the end (Vergniolle and Caplan-Auerbach 2004).

The temporal evolution of gas volume emitted at the surface by the hum events exhibits a clear rupture between 12h00 and 14h00 (Vergniolle and Caplan-Auerbach 2004). Around that time, the number of detected hum events is very small (Fig. 9a) and of low amplitude, ≈1 Pa. At ≈13h06, one of the largest intermittencies between successive hum events, ≈600 s occurs (Vergniolle and Caplan-Auerbach 2004).

We have repeated the same analysis using stacks calculated on fifteen minutes instead of thirty minutes (Fig. 9) and found similar results with an improved time accuracy. The match between synthetic waveforms (Vergniolle and Caplan-Auerbach 2004) and recorded hum events is poor between 13h15 and 13h45 due to the small number of hum events (Fig. 9a). Nevertheless, gas overpressure and intermittency between hum shows a clear rupture between 13h15 and 13h45 (Fig. 9b and 9c). The evolution of the intermittency averaged over 15 minutes is very similar for the period from 6h45 to 11h30 and from 13h30 to 19h30 (Fig. 9c), suggesting that something major has happened between 11h30 and 13h30.

Low frequency signals, below 0.5 Hz, become particularly energetic between ≈12h21 and ≈12h30 (Fig. 10). As with other signals recorded by the pressure sensor, we first considered the possibility that the signal had a source that was unrelated to the volcano. Again, wind conditions at the site were unknown but wind recorded 92 km away was mild at the time. The seismic signal, however, did not show the broadband noise generally associated with wind, nor was significant microbarometric noise, ≈0.2 Hz (Kibblewhite and Wu 1996), evident. Furthermore, the low-frequency signal occurs at a time with few hum events or bubble bursts signals (Vergniolle and Caplan-Auerbach 2004). Because this represents a significant change in the acoustic record, we assume that the low-frequency signal also results from a volcanic process. We note that no significant signal was recorded on seismometers at this time, suggesting that the signal was not energetic and may have had a shallow source.

The combination of a hiatus in hum events and the presence of the low frequency signal described above suggests that there was a change in eruption dynamics at this time. We propose that these changes are due to the formation of a thermal during the pre-Subplinian phase, referred later in the text as the first thermal phase.

While a plume corresponds to the continuous release of gas and magma in the atmosphere, a thermal is characterised by the quasi-instantaneous release of gas and magma (Turner 1973; Sparks et al. 1997). Because the

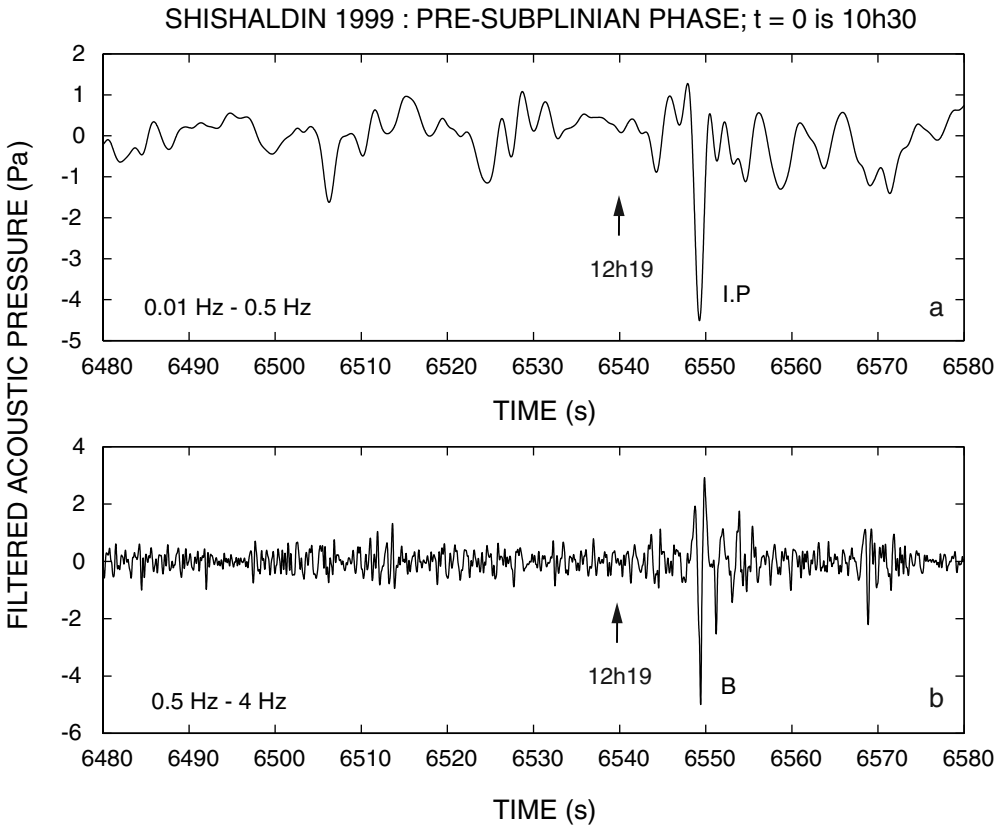

Fig. 11 Acoustic pressure (Pa), around the first thermal phase, as a function of time (s) andfiltered with a zero phase lag filter to ensure a correct time. **a** Filtering, between 0.01 Hz and 0.5 Hz, is used to detect the beginning of the thermal phase. I.P. (Initial Pulse) marks the potential location where the thermal phase starts, as given from the gas velocity method (Fig. 12). **b** Filtering, between 0.5 Hz and4 Hz, is used to detect large bubble breaking, marked B. The bubble B, at ≈12h19 (6548 s) is the equivalent of the trigger bubble of the Subplinian phase and occurs at the start of the thermal

thermal is not supported by the continuous addition of hot material with momentum from below, it rises in the atmosphere to significantly lower heights than does a plume, hence can go undetected under the cloud cover.

A trigger bubble for the first thermal phase

When the pressure record around the time of the first thermal phase is highpass filtered above 0.5 Hz (Fig. 11), waveforms similar to those generated by the breaking of large overpressurised bubbles during Strombolian eruptions are observed. In that case, the sound is produced by the vibration of an overpressurised bubble at the top of the magma column (Vergniolle and Brandeis 1994; Vergniolle and Brandeis 1996; Vergniolle et al. 1996; Ripepe and Gordeev 1999; Vergniolle et al. 2004). Details of the modelling of these events can be found in another paper (Vergniolle et al. 2004). For the Strombolian events, we assumed that the magma above the bubble has a constant thickness of h_{eq} ≈0.15 m. In these conditions, the bubble radius, length and overpressure are respectively 3.5 m, 240 m, 0.06 MPa at ≈12h19 and 3.5 m, 160 m, 0.07 MPa at ≈12h25 because they rise in a foam (Eq. (13)).

The general evolution of the gas velocity suggests that the thermal phase starts at ≈6550 ± 5 s (Fig. 12, see below). Acoustic pressure, filtered below 0.5 Hz, shows a signal at that time (I.P. in Fig. 11), which is the strongest event of that period and hence could be considered as the beginning of the thermal phase. Therefore, we suggest that the bubble at 12h19, which occurs at the initiation of the thermal phase, is the analog of the Subplinian trigger bubble (Vergniolle and Caplan-Auerbach 2004) despite its smaller overpressure. In that case, the initiation of the first thermal phase is simultaneous tothe breaking of its trigger bubble at the surface (Fig. 11), whereas the initiation of the Subplinian phase occurs ≈28 s ahead of its trigger bubble (Fig. 6c).

Gas velocity at the vent for the first thermal phase

We further examine the low-frequency signal between 12h15 and 12h30 by calculating the gas velocity at that time, assuming a dipole source (Eq. (10)), as for the Subplinian phase. By analogy to the Subplinian phase, a thermal or a plume starts to form at the vent when a large overpressurised bubble approaches and breaks the top of the magma column after which the gas velocity decreases almost linearly. We can recognize this trend at ≈12h25, and two possible events at ≈12h19 and ≈12h22mn30s(Fig. 12). However, the short total duration, ≈643 s (Table 2) relative to the duration of the Subplinian phase (≈2806 s), places this event in the domain of a thermal rather than a plume. As with the Subplinian phase, each thermal is separated by a "decompression" phase, characterised by a linear increase in gas velocity. The two large peaks in gas velocity (B in Fig. 12) at ≈12h19 and ≈12h25 are overestimates resulting from the use of a dipole model for the two

Table 2 Estimates for the first thermal phase, observed during the pre-Subplinian phase at 12h19, and composed by a trigger thermal (0th) and the two "plumes" (1 to 2). Time equal 0 refers to 10h30 and real time are respectively 12h19mn10s, 12h21mn59s, 12h25mn40s. Gas velocity is calculated by using Eq. ((3.10)) with a constant K_d of 1/3 and a vent area based on a conduit radius of ≈6 m (Vergniolle et al. 2004]. Mean is the mean value for the two "plumes" or "decompressions" without the trigger thermal. Std means standard deviation, Vol means volume and Vel means measured velocity. Aver means average, Max maximum and Min minimum. Slope is the decrease of measured gas velocity in time. Decompression time of plume 1 is the time between plume 1 and 2, and right after plume 1. Gas volume used for calculating gas flux is the gas volume expelled during the trigger thermal (0) and the two "plumes" (1 to 2). Gas flux is based on the total duration of the thermal (0) and two "plumes" (1 and 2) and the three "decompression periods

Plume	0th	1st	2nd	Mean	Std	Tot
Time (s)	6550	6719	6940			
Duration (s)	58	129	253	191	88	643
Aver.Veloc ($m.s^{-1}$)	82	90	85	88	3.3	
Max.Veloc ($m.s^{-1}$)	87	99	100	99	0.41	
Min.Veloc ($m.s^{-1}$)	77	81	71	76	6.9	
Slope ($\times 10^{-2} m.s^{-2}$)	16	14	11	13	2	
Gas Vol ($\times 10^6 m^3$)	0.54	1.3	2.5	1.9	0.8	4.30
Gas Flux ($\times 10^3 m^3/s$)	9.3	10	9.7	9.9	3.7	6.7
Decompression	0th	1st	2nd	Mean	Std	Tot
Dec. Time (s)	6608	6648	7194			
Duration (s)	111	92	323			
Height (km)	1.8	2.2	2.6	2.4	0.26	3.0

monopole bubble bursting signals (Eqs. (4) and (10)). If we discard the two peaks in gas velocity which correspond to the two large gas bubbles at ≈12h19 and ≈12h25, the calculated gas velocity between 12h18 and 12h30 is rather large, ≈88 m/s (Fig. 12, Table 2). This is also in the range of exit velocities measured during Vulcanian explosions, between 40 and 140 m/s at Soufrière Hills (Druitt et al. 2002).

A second thermal phase during the pre-subplinian phase

Because direct observations detected a small "plume" at 13h20 in the atmosphere, the gas velocity was calculated from acoustic power for the period 12h30-13h20. At 13h12, acoustic measurements show an event very similar to the triggering event of the first thermal phase at 12h19 (Fig. 11). Furthermore, gas velocity presents a time series very analogous to the first thermal phase (12h19-12h30), suggesting the formation of a thermal at the vent. The total gas volume, ejected between 13h12 and 13h21, is ≈3.6 $10^6 m^3$ and other results are summarised in Table 3.

Although thermal phases initiate with only a moderately overpressurised bubble, ≈0.06 MPa for the first thermal phase, it still represents a classical Vulcanian explosion/thermal. Consequently Shishaldin displayed a wide variety of basaltic activity during its 1999 eruption, including Strombolian explosions, Vulcanian explosion/thermal, and a Subplinian plume. There is also a continuum during the pre-Subplinian phase towards increasing the strength of the eruption (Vergniolle and Caplan-Auerbach 2004), until it reaches its climax, i.e. during the Subplinian plume.

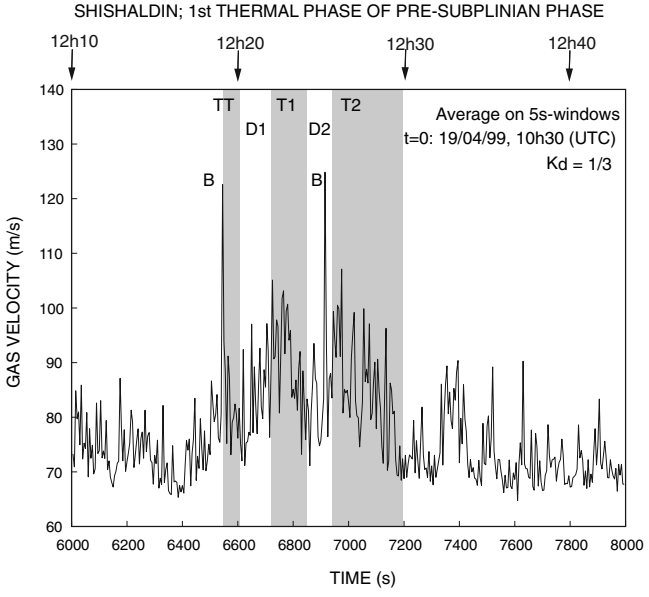

Fig. 12 Gas velocity (m/s) as estimated (Eq. (10)) using acoustic power averaged over a 5 s duration with a constant $K_d = 1/3$, avent area based on a conduit radius of ≈6 m (Vergniolle et al. 2004) and assuming a dipolar sound radiation. B marks where thegas velocity is overestimated, because the signal corresponds to a bubble bursting, a monopole source. TT, T1 and T2 are respectivelythe trigger thermal, and the two successive thermals of the first thermal phase at 12h19–12h30. D1 and D2 are the two decompression periods

Independent estimates of gas flux

Gas flux from the plume height

Finally, we use the gas velocity to estimate gas flux and gas volume and compare it with models of plume rise in

Table 3 Estimates for the second thermal phase, observed during the pre-Subplinian phase at 13h12, and composed by the trigger thermal (0) and the three "plumes" (1 to 3). Time equal 0 refers to 10h30 and real time are respectively13h12mn19s, 13h15mn27s, 13h17mn56s and 13h19mn29s. Gas velocity is calculated by using Eq. ((3.10)) with a constant K_d of 1/3 and a vent area based on a conduit radius of ≈6 m (Vergniolle et al. 2004). Mean is the mean value for the five "plumes" or "decompressions" without the trigger thermal. Std means standard deviation, Tot represents the case of a single foam in the conduit, Vol means volume and Vel means velocity, Aver means average and Max maximum. Slope is the decrease of measured gas velocity in time. Decompression time of plume 1 is the time between plume 1 and 2, and right after plume 1. Gas flux is based on the total duration of the four "plumes" and the four "decompression" periods (see text for details). Note that the calculated height, ≈2.8 km, is in very good agreement with the observation of a small plume at the vent at 13h20

Plume	0th	1st	2nd	3rd	Mean	Std	Tot
Time (s)	9742	9927	10076	10168			
Duration (s)	130	50	64	85	66	18	511
Aver.Veloc (m.s^{-1})	99	93	92	93	93	0.60	
Max.Veloc (m.s^{-1})	110	100	100	100	100	0.34	
Min.Veloc (m.s^{-1})	86	84	83	85	84	1.2	
Slope ($\times 10^{-2}$m.s^{-2})	21	36	29	19	28	8.0	
Gas Vol ($\times 10^6$m^3)	1.5	0.53	0.67	0.90	0.70	0.19	3.55
Gas Flux ($\times 10^3$m^3/s)	11	11	10	11	11	0.7	6.9
Decompression	0th	1st	2nd		Mean	Std	Tot
Time (s)	9872	9977	10140	10253			
Duration (s)	55	99	28	147	82.2	52.1	
Height (km)	2.3	1.8	1.9	2.0	1.9	0.13	2.8

atmosphere. Gas flux at the surface Q_{gvent} can be estimated from the gas velocity U and the area of a vent of radius R_c. After the eruption, in August 1999, the vent radius was observed to be ≈12–15 m (Vergniolle et al. 2004). However because flaring of the vent is a very common feature, and because the vent was partly widened during the eruption (P. Stelling, pers. com. 2002), we use the estimate from acoustic measurements of $R_c \approx 6$ m (Vergniolle et al. 2004). Furthermore this radius of ≈6 m corresponds exactly to the top of the magma column, which is the location where the plume initiates:

$$Q_{\text{gvent}} = U \pi R_c^2 \cdot \tag{19}$$

Mean gas velocity during the first thermal phase is ≈88 ± 3.3 m/s (Fig. 12, Table 2) for surficial gas flux estimates of $\approx 0.99 \times 10^4 \pm 0.37 \times 10^4$ m^3/s (Table 2). Although these values are very similar to gas flux emitted during the Subplinian phase, $\approx 0.93 \times 10^4 \pm 0.33 \times 10^4$ m^3/s, their short durations, for a total of ≈643 s, suggest that their behaviour is that of a thermal, where gas is not continuously fed at the source.

Gas volume at atmospheric pressure can be calculated from the gas flux, knowing that the duration of the three pulses are ≈58 s, ≈129 s, and ≈253 s. Gas volume for each pulse is found to be $1.9 \times 10^6 \pm 0.8 \times 10^6$ m^3 (Table 2).

The distinction between a plume and a thermal has a dramatic effect on the height of the erupted material. For the thermal, its height H_T in the atmosphere depends on its initial volume V_{T0} and on its temperature contrast (Sparks et al. 1997):

$$H_{\text{T}} = 2.6\ F_{\text{T}}^{1/4}\ N^{-1/2} \tag{20}$$

where N is the Brunt-Väisälä frequency, i.e. the frequency of internal gravity waves in the stratified atmosphere (Lighthill 1978) and ranges between 5×10^{-3} Hz and 10^{-2} Hz for a typical atmosphere (Sparks et al. 1997). F_{T} is defined as:

$$F_{\text{T}} = V_{\text{T0}}\, g\ \frac{T_{\text{T0}} - T_{\text{atm}}}{T_{\text{atm}}}. \tag{21}$$

T_{T0} is the initial temperature of the mixture, ≈1323 K (Stelling et al. 2002), T_{atm} the ambient temperature, ≈273 K.

In contrast, the height of a plume, continuously fed by gas at the source, depends on gas flux at the source. An empirical, therefore very approximate, relationship, which relates the height of the plume, H_{plume} in km, to its gas flux at the surface, Q_{gvent} in m^3/s, has been widely used in volcanology because of its simplicity (Sparks et al. 1997), giving:

$$Q_{\text{gvent}} = \left[\frac{H_{\text{plume}}}{1.67}\right]^{\frac{1}{0.259}}. \tag{22}$$

Gas flux during the first thermal phase

For the three phases of the first pre-Subplinian thermal phase, use of Eq. (21) yields approximate heights in the atmosphere of ≈2.4 ± 0.26 km. If instead we consider the possibility that these events were continuously gas-fed despite their short duration and use Eq. (22), we find that their

expected heights would be closer to 18 km. Although the area was clouded at the time of the pre-Subplinian phase, a plume of this height would have been easily visible in satellite imagery. Results are similar for the second thermal phase (Table 3). The fact that only a small plume was observed at 13h20 on April 19 is strong evidence that these features formed as thermals.

Gas flux during the Subplinian phase

As for the pre-Subplinian phase, we take the radius of the vent to be 6 m (Vergniolle et al. 2004) and calculate gas flux according to Eq. (19). Mean gas velocity during the five "plumes" is $\approx 82 \pm 3.2$ m/s, (Fig. 3), leading to a mean gas flux of $\approx 0.93 \times 10^4 \pm 0.33 \times 10^4$ m^3/s (Table 1).

Gas volume at atmospheric pressure can be calculated from the gas flux, knowing the duration of the five "plumes," $\approx 309 \pm 105$ s. The total gas volume is equal to $\approx 1.5 \times 10^7$ m^3 if we consider the five plumes plus the trigger thermal and 2.9×10^7 m^3 if we include the gas expelled during the six "decompression" phases. However since the "decompression" periods may not correspond to the expulsion of gas at the vent, we first ignore their gas volume. This value is greater than estimates of 3.2×10^6 m^3 for the Subplinian eruption of Soufrière Hills (Montserrat) (Robertson et al. 1998).

Use of Eq. (22) allows us to estimate gas flux at $6.1 \times 10^3 m^3/s$ for the observed plume height of 16 km (Nye et al. 2002), corresponding to two thirds of the gas flux estimated from acoustic measurements for the each period of the Subplinian phase Eq. (19). If we calculate the height reached by a plume fed by a gas flux equivalent to the one measured by acoustic measurements, we obtain 17.8 km. The discrepancy between the two estimates Eqs. (19) and (22), 16 km versus 17.8 km, can be due either to inaccurate approximations in Eq. (22) or to inaccurate estimates of the plume height. Plume height was estimated from satellite data, which shows that the plume is strongly sheared when it enters the stratosphere, at $\approx$16 km. Therefore in the absence of shearing, it might be expected that the plume would rise higher, suggesting that acoustic data give a good estimate of the gas flux produced by the volcano. The second factor of discrepancy may come from the value of the coefficient K_d Eq. (10). The use of K_d equal to 0.013 (Woulff and McGetchin 1976) has been shown to overestimate gas velocity, gas flux and gas volume by a factor 1.7, leading to a plume height of 20.4 km. This large difference with observation suggests that the choice of K_d, based on Eqs. (5) to (9) and equal to 1/3, is the most appropriate. The very good agreement between gas flux from plume height and from acoustic measurements also reinforces our choice of the periods corresponding to the upwards motion of gas and ejecta.

If we had included the six "decompression" periods as significant of an upper motion of gas at the vent, the plume height would be 19 km. This overestimation, compared to the observed minimum height of 16 km, suggests that "decompression" periods correspond to relatively quiet periods, in which gas velocity cannot be estimated by the dipole approximation. Hence, we propose that the "decompression" periods do not contribute significantly to the ejected gas volume.

Conclusion

Acoustic measurements provide a quantitative understanding of the eruption dynamics of the 1999 eruption of Shishaldin volcano. The Subplinian phase is composed of six periods during which the motion of gas and magma is upwards. Although the acoustic waveform produced by a volcanic plume or thermal is complex, use of acoustic power allows us to estimate gas velocity and total gas volume at $\approx$82 m/s and $\approx 1.5 \times 10^7$ m^3 for a mean gas flux of $\approx 0.93 \times 10^4$ m^3/s. The analysis of the Subplinian phase has shown that its start is related to the arrival of a large overpressurised bubble at the vent. Then gas velocity displays a specific trend, in which it alternates between periods marked by an initial jump followed by a regular decrease and periods showing an increase.

We believe that two thermal phases formed in the middle of the pre-Subplinian phase. These thermals, which could also be called a Vulcanian explosion/plume, represents an eruption midway between the explosive Subplinian activity and the relatively "mild" Strombolian explosions which also occurred in the 1999 eruption. Thus, although lava and pyroclastic flows were notably absent, the 1999 eruption exhibited a continuum of types of eruptive activity. The data presented here confirm that acoustic records can provide a wealth of information on eruption mechanics, even for a case where visual observations are lacking. The similarity in gas velocity and gas flux between the thermal phases of the pre-Subplinian phase and the Subplinian phase suggests that their formation results from the same mechanism.

There is also an excellent agreement between gas flux calculated from acoustic pressure with that estimated from the plume height. Hence, measuring the sound produced by volcanoes is a very robust method to quantify the erupted gas volume and gas flux at the vent.These are the primary physical parameters responsable for surface activity, hence implementing acoustic measurements on erupting volcanoes can be a very valuable method for volcano monitoring.

Acknowledgments We warmly thank Milton Garcés for taking the initiative to install a pressure sensor at Shishaldin. We also thank Matthias Hort and the two anonymous reviewers. This work was supported by CNRS-INSU (ACI and PNRN: Contribution number 369) and by the French Ministère de l'Ecologie et Développement Durable (Numbers: 265 and 281). This is IPGP contribution number 2915.

References

Alidibirov MA (1994) A model for viscous magma fragmentation during volcanic blasts. Bull Volcanol 56:459–465.

Andres RJ, Rose WI (1995) Remote sensing spectrometry of volcanic plumes and clouds. In: McGuire WJ, Kilburn C, Murray J (eds) Monitoring active volcanoes. University College London, London.

Batchelor GK (1967) An introduction to fluid dynamics. Cambridge University Press, Cambridge.
Beget J, Nye C, Stelling P (1998) Postglacial collapse and regrowth of Shishaldin volcano, Alaska, based on historic and prehistoric tephrochronology. Eos Trans Am Geophys Union 79:F979
Buckingham MJ, Garcés MA (1996) A canonical model of volcano acoustics. J Geophys Res 101:8129–8151
Caplan-Auerbach J, McNutt SR (2003) New insights into the 1999 eruption of Shishaldin volcano based on acoustic data. Bull Volcanol 65:405–417
Carey S, Sigurdsson H, Gardner JE, Criswell W (1990) Variations in column height and magma discharge during the May 18, 1980 eruption of Mount St-Helens. J Volcanol Geotherm Res 43:99–112
Chouet B, Hamisevicz N, McGetchin TR (1974) Photoballistics of volcanic jet activity at Stromboli, Italy. J Geophys Res 79:4961–4975
Coltelli M, Del Carlo P, Vezzoli L (1995) Stratigraphy of the Holocene Mt. Etna explosion eruptions. Periodico di Mineralogia 64:141–143
Coltelli M, Del Carlo P, Vezzoli L (2000) Stratigraphic constraints for explosive activity in the past 100 ka at Etna volcano, Italy. Int J Earth Sci 89:665–677
Dehn J, Dean KG, Engle K, Izbekov P (2002) Thermal precursors in satellite images of the 1999 eruption of Shishaldin Volcano. Bull Volcanol 64:525–534
Druitt TH, Young SR, Baptie B, Bonadonna C, Calder ES, Clarke AB, Cole PD, Harford CL, Herd RA, Luckett R, Ryan G, Voight B (2002) Episodes of cyclic Vulcanian explosive activity with fountain collapse at Soufrière Hills Volcano, Montserrat. In: Druitt TH, Kokelaar BP (eds) The eruptions of Soufrière Hills Volcano, Montserrat, from 1995 to 1999. Geol Soc London Mem 21:281–306
Dubosclard G, Cordesses R, Allard P, Hervier C, Coltelli M, Kornprobst J (1999) First testing of a volcano Dopler radar (Voldorad) Mat Mount Etna, Italy. Geophys Res Lett 26:3389–3392
Dubosclard G, Donnadieu F, Allard P, Cordesses R, Hervier C, Coltelli M, Privitera E, Kornprobst J (2004) Doppler radar sounding of volcanic eruption dynamics at Mount Etna. Bull Volcanol 66 5:443–456
Fabre J, Linné A (1992) Modelling of two-phase slug flow. Ann Rev Fluid Mech 24:21–46
Garcés MA, McNutt SR (1997) Theory of the airborne sound field generated in a resonant magma conduit. J Volcanol Geotherm Res 78:155–178
Hagerty MT, Schwartz SY, Garcés MA, Protti M (2000) Analysis of seismic and acoustic observations at Arenal Volcano, Costa Rica, 1995–1997. J Volcanol Geotherm Res 101:27–65
Hoblitt RP, Wolfe EW, Scott WE, Couchman MR, Palister JS, Javier D (1996) The pre-climatic eruptions of Mount Pinatubo, June 1991. In: Newhall CG, Punongbayan RS (eds) Fire and mud: eruptions and lahars of Mount Pinatubo, Philippines. University of Washington Press, Seattle.
Hort M, Seyfried R (1998) Volcanic eruption velocities measured with a micro radar. Geophys Res Lett 154:515–532
Hort M, Seyfried R, Vöge M (2003) Radar Doppler velocimetry of volcanic eruptions: Theoretical considerations and quantitative documentation of changes in eruptive behaviour at Stromboli volcano, Italy. Geophys J Int 25 1:113–116
Houghton BF, Wilson CJN, Del Carlo P, Coltelli M, Sable JE, Carey R (2004) The influence of conduit processes on changes in style of basaltic Plinian eruptions: Tarawera 1986 and Etna 122 BC. J Volcanol Geotherm Res 137:1–14
Johnson MC, Anderson AT, Rutherford MJ (1994) Pre-eruptive volatile contents in magmas. In: Carroll MR, Holloway JR (eds) Volatiles in magmas. Mineral Soc of Am Washington D.C, pp 281–330
Johnson JB, Lees JM, Gordeev EI (1998) Degassing explosions at Karymsky Volcano, Kamchatka. Geophys Res Lett, 25:3999–4002
Johnson JB, Lees JM (2000) Plugs and chugs: seismic and acoustic observations of degassing explosions at Karymsky, Russia and Sangay, Ecuador. J Volcanol Geotherm Res 101:67–82
Kanamori H, Mori J (1992) Harmonic excitation of mantle Rayleigh waves by the 1991 eruption of mount Pinatubo, Philippines. Geophys Res Lett 19:721–724
Kaminski E, Jaupart C (2001) Marginal stability of atmospheric eruption columns and pyroclastic flow generation. J Geophys Res 106, B10:21,785–21,798
Kibblewhite AC, Wu CY (1996) Wave interactions as a seismoacoustic source. Lecture Notes in Earth Sciences, Springer-Verlag, Berlin
Kinsler LE, Frey AR, Coppens AB, Sanders JV (1982) Fundamentals of acoustics. John Wiley and Sons, New York
Klein FW, Koyanagi RY, Nakata JS, Tanigawa WR (1987) The seismicity of Kilauea's magma system. US Geol Surv Prof Paper 1350:1019–1186
Laigle M., Hirn A (1999) Explosion-seismic tomography of a magmatic body beneath Etna: volatile discharge and tectonic control of volcanism. Geophys Res Lett 26: 17:2665–2668
Laigle M, Hirn A, Sapin M, Lepine J-C (2000) Mount Etna dense array local earthquake P and S tomography and implications for volcanic plumbing. J Geophys Res 105: 21633–21646
Landau LD, Lifshitz EM (1987) Course in theoretical Physics, 6 : fluids mechanics. Pergamon Press, Oxford
Leighton TG (1994) The acoustic bubble. Academic Press, London
LePichon A, Blanc E, Drob D, Lambotte S, Dessa JX, Lardy M, Bani P, Vergniolle S (2005) Continuous infrasound monitoring of volcanoes to probe high-altitude winds, J Geophys Res 110: D13106, DOI: 1029/2004JD005587
Lighthill J (1978) Waves in fluids. Cambridge University Press Cambridge
McGetchin TR, Settle M, Chouet B (1974) Cinder cone growth modeled after northeast crater, Mount Etna, Sicily. J Geophys Res 79: 23:3257–3272
Mader HM, Phillips JC, Sparks RSJ, Sturtevant B (1996) Dynamics of explosive degassing of magma: observations of fragmenting two-phase flows. J Geophys Res 101: 5547–5560
Mader HM (1998) Conduit flow and fragmentation. In: Gilbert JS, Sparks RSJ (eds) The physics of explosive volcanic eruptions. Geo Soc London Spec Pub 145:51–71
Massol H, Jaupart C (1999) The generation of gas overpressure in volcanic eruptions. Earth Planet Sci Lett 166:57–70
Morrissey MM, Chouet B (1997a) A numerical investigation of choked flow dynamics and its application to the triggering-mechanism of long-period events at Redoubt Volcano, Alaska. JGeophys Res 102:7965–7983
Morrissey MM, Chouet B (1997b) Burst conditions of explosive volcanic eruptions recorded on microbarographs. Science 275:1290–1293
Nye CJ, Keith T, Eichelberger JC, Miller TP, McNutt SR, Moran SC, Schneider DJ, Dehn J, Schaefer JR (2002) The 1999 eruption of Shishaldin volcano, Alaska: monitoring a distant eruption. Bull Volcanol, 64:507–519
Phillips JC, Lane SJ, Lejeune AM, Hilton M (1995) Gum rosin-acetone system as an analogue to the degassing behaviour of hydrated magmas. Bull Volcanol 57:263–268
Ripepe M, Rossi M, Saccarotti G (1993) Image processing of explosive activity at Stromboli. J Volcanol Geotherm Res 54:335–351
Ripepe M, Gordeev E (1999) Gas bubble dynamics model for shallow volcanic tremor at Stromboli. J Geophys Res 104:10,639–10,654
Robertson R, Cole P, Sparks RSJ, Harford C, Lejeune AM, McGuire WJ, Miller AD, Murphy MD, Norton G, Stevens NF, Young SR (1998) The explosive eruption of Soufriere Hills Volcano, Montserrat, West Indies, 17 September, 1996. Geophys Res Lett 25: 18:3429–3432
Ryan MP (1988) The mechanics and three-dimensional internal structure of active magma systems: Kilauea volcano, Hawaii. J Geophys Res 93:4213–4248
Schmincke H-U (2004) Volcanism. Springer-Verlag, Berlin Germany, pp 1–324

Sisson TW, Grove TL (1993) Temperatures and H_2O contents of low-MgO high-aluminia basalts. Contrib Mineral Petrol 113:167–184

Sparks RSJ, Bursik MI, Carey SN, Gilbert JS, Glaze LS, Sigurdsson H, Woods, John AW (1997) Volcanic plumes. John Wiley and Sons, Chichester.

Stelling P, Beget J, Nye C, Gardner J, Devine JD, George RMM (2002) Geology and petrology of ejecta from the 1999 eruption of Shishaldin Volcano, Alaska. Bull Volcanol 64:548–561

Temkin S (1981) Elements of acoustics. John Wiley and Sons, Chichester

Thompson G, McNutt SR, Tytgat G (2002) Three distinct regimes of volcanic tremor associated with the eruption of Shishaldin volcano, Alaska, April 1999. Bull Volcanol 64:535–547

Turner JS (1973) Buoyancy effects in fluids. Cambridge University Press, Cambridge.

Vergniolle S, Brandeis G (1994) Origin of the sound generated by Strombolian explosions. Geophys Res Lett 21:1959–1962

Vergniolle S, Brandeis G (1996) Strombolian explosions: A large bubble breaking at the surface of a lava column as a source of sound. J Geophys Res 101:20,433–20,448

Vergniolle S, Brandeis G, Mareschal J-C (1996) Strombolian explosions: Eruption dynamics determined from acoustic measurements. J Geophys Res 101:20,449–20,466

Vergniolle S (1998) Modelling two-phase flow in a volcano. Proc 13th Australasian Fluid Mech Conf Aristoc Offset, Monash University, Melbourne, p647–650

Vergniolle S (2001) Listening to Stromboli volcano as a tool into its volcanic conduit. Eos Trans Am Geophys Union 82, 47:F1399

Vergniolle S, Boichu M, Caplan-Auerbach J (2004) Acoustic measurements of the 1999 basaltic eruption of Shishaldinvolcano, Alaska: 1) Origin of Strombolian activity. J Volcanol Geotherm Res 137:109–134

Vergniolle S, Caplan-Auerbach J (2004) Acoustic measurements of the 1999 basaltic eruption of Shishaldin volcano, Alaska: 2) Precursor to the Subplinian activity. J Volcanol Geotherm Res 137:135–151

Vergniolle S, Caplan-Auerbach J (2005) Foam disruption as the origin of the Subplinian, basaltic plume at Shishaldin volcano (Alaska). J Geophys Res subm.1

Vergniolle S, Caplan-Auerbach J (2005) Insights into magma chamber behaviour at Shishaldin volcano from the chronology of the 1999 eruption J Geophys Res subm.2

Walker GPL, Self S, Wilson L (1984) Tarawera 1886, New Zealand–a basaltic Plinian fissure eruption. J Volcanol Geotherm Res 21:61–78

Wallace P, Anderson AT (2000) Volatiles in magma. Encyclopedia of Volcanoes, Academic Press, San Diego

Wallace P (2005) Volatiles in subduction zone magmas: concentrations and fluxes based on melt inclusion and volcanic gas data. J Volcanol Geotherm Res 140:217–240

Wallis GB (1969) One dimensional two-phase flows. Mc Graw Hill, New York

Weill A, Brandeis G, Vergniolle S, Baudin F, Bilbille J, Fevre J-F, Piron B, Hill X (1992) Acoustic sounder measurements of the vertical velocity of volcanic jets at Stromboli volcano. Geophys Res Lett 19:2357–2360

Williams SN (1983) Plinian airfall deposits of basaltic composition. Geology 11:211–214

Woulff G, McGetchin TR (1976) Acoustic noise from volcanoes: Theory and experiments. Geophys J R Astron Soc 45:601–616

Zhang Y, Sturtevant B, Stolper EM (1997) Dynamics of gas-driven eruptions: experimental simulations using CO_2-H_2O-polymer system. J Geophys Res 102:3077–3096